International Journal of Mechanical System Dynamics

WILEY

IJMSD International Journal of Mechanical System Dynamics Open Access

RESEARCH ARTICLE OPEN ACCESS

Dynamic Behavior of a Two-Degree-of-Freedom System With Electromagnetic Interaction via a Skew-Symmetric Matrix

Fernando Cortés[1] | Ondiz Zarraga[2] | Julen Cortazar-Noguerol[1] | Imanol Sarría[1] | María Jesús Elejabarrieta[1]

[1]Department of Mechanics, Design and Industrial Management, University of Deusto, Bilbao, Spain | [2]Department of Mechanical and Industrial Production, Mondragon Unibertsitatea, Mondragon, Spain

Correspondence: Fernando Cortés (fernando.cortes@deusto.es)

Received: 26 May 2025 | **Revised:** 21 July 2025 | **Accepted:** 27 July 2025

Funding: This study was supported by the Department of Education of the Basque Government for the Research Group program IT1507–22.

Keywords: frequency splitting in conservative systems | mechanical-electromagnetic mode coupling | non-orthogonal modes | skew-symmetric interaction matrix | time and frequency response

ABSTRACT

This paper analyzes the dynamic behavior of a two-degree-of-freedom system subjected to electromagnetic interaction modelled through a skew-symmetric coupling matrix. The system comprises two mechanically independent oscillators coupled by velocity-dependent electromagnetic forces. The equations of motion are formulated and analyzed in the modal domain, highlighting the effects of the antisymmetric interaction on natural frequencies and mode shapes. The classical orthogonality is broken, resulting in complex eigenvectors; nevertheless, the system remains conservative, as the interaction forces perform no work. The analysis is carried out using both configuration-space and state-space formulations, revealing modal frequency splitting and phase shifts induced by the skew-symmetric term. These modal features are further examined through time-domain simulations and frequency response functions. The main contribution of this study is the development and analysis of a deliberately simple yet general model that isolates the essential dynamic effects of skew-symmetric electromagnetic coupling. This minimal formulation, often hidden in more complex systems, reveals key phenomena such as modal frequency splitting, non-normal modes, and energy-conserving cross-effects. The model serves not only as a conceptual reference but also as a methodological framework applicable to a broad class of coupled electromechanical systems.

1 | Introduction

The interaction between mechanical and electromagnetic fields refers to the interdependence of these two fundamental aspects of physics. It arises when changes in mechanical systems induce changes in electromagnetic fields, or vice versa, creating a dynamic relationship that significantly influences the behavior and properties of physical systems. Understanding this interaction is crucial across disciplines such as electrical and mechanical engineering, materials science, and physics, as it underpins the operation of numerous devices and systems including motors, generators, sensors, actuators, and transducers.

On the one hand, in electrical engineering, the integration of mechanical, and electromagnetic principles is fundamental to the design, operation, and performance of electrical machines [1]. From generators and motors [2–4] to transformers [5] and actuators [6], these machines rely on the complex interaction between mechanical motion and electromagnetic forces. For instance, in rotating machines like motors and generators, mechanical motion induces

changes in magnetic flux, leading to the generation of electromotive forces (EMFs) and electrical currents. Conversely, the interaction of electrical currents with magnetic fields generates forces and torques on mechanical components, driving rotational motion or producing mechanical outputs. This bidirectional interplay between the mechanical and electromagnetic domains governs the performance and efficiency of electrical machines.

On the other hand, in mechanical engineering, a prominent application of this interaction is eddy current damping [7], as seen in magnetic brakes [8], seismic dampers [9], and lever-type vibration isolators [10]. Several studies [11, 12] have reviewed these varied applications in detail. Furthermore, in energy harvesting systems, piezoelectric beams operating within electromagnetic fields [13–15] experience coupling forces that alter their mechanical behavior.

Another key example are microelectromechanical systems (MEMS), which exemplify the seamless integration of mechanical and electromagnetic principles, addressing several engineering challenges. In MEMS, mechanical components undergo elastic vibrations [16–18], such as the bending of electrostatically charged beams [19–22] and sandwich composites [23], while electromagnetic fields exert forces and torques on these structures, influencing their mechanical responses.

Recent advances in the study of nonsymmetric coupling and vibrational dynamics have been reported in several works. These studies analyze the impact of complex mechanical, magnetic, and electromechanical couplings on the modal properties, stability, and bifurcation scenarios of multi-degree-of-freedom systems. For instance, Amer et al. have investigated the resonance and stability of triple and double pendulum systems under various excitations, employing advanced analytical and numerical techniques to reveal transitions between periodic, quasiperiodic, and chaotic behaviors [24, 25]. Other works extend these approaches to systems with piezoelectric harvesters and magnetic absorbers, highlighting practical implications for energy harvesting and vibration control [26, 27]. Additionally, recent analyses of magnetic inverted and spherical pendulums provide insights into the stabilizing role of magnetic fields and the influence of nonconservative forces [28, 29]. Unlike these previous studies, the present work introduces a minimalist analytical model that isolates the effects of skew-symmetric electromagnetic coupling, enabling a detailed exploration of frequency splitting and non-orthogonality in a conservative framework.

The paper is organized as follows: after the introduction in Section 1, the system definition and governing equations are presented in Section 2. The eigenvalue problem is then solved using two approaches: the configuration-space and state-space formulations, with eigenvalues, eigenvectors, and their orthogonality and normalization properties analyzed in both cases. Sections 4 and 5 address the free vibration and harmonic response of the system, respectively, employing both approaches. Section 6 presents a numerical application, and finally, Section 7 summarizes the main conclusions.

2 | System Definition and Governing Equations

In this section, the equations of motion for an electrostatically charged body vibrating in a magnetic field are developed. Figure 1A illustrates the body of mass m and electrostatic charge q vibrating in the horizontal x-y plane. A magnetic field with flux density $\boldsymbol{B} = B\,\boldsymbol{z}$ is applied, where $\boldsymbol{z}$ is the unit vector in the z direction (perpendicular to the x-y plane) and B is the magnitude of the magnetic flux density. The body is connected to the ground by two springs aligned with the x and y directions, the stiffness constants of the springs being k_x and k_y, respectively. The position vector $\boldsymbol{u}(t)$ of the body is given by $\boldsymbol{u}(t) = [x(t) \quad y(t)]^{\mathrm{T}}$, where the superscript $(\cdot)^{\mathrm{T}}$ denotes the transpose operator. The corresponding velocity and acceleration vectors are $\dot{\boldsymbol{u}}(t) = [\dot{x}(t) \quad \dot{y}(t)]^{\mathrm{T}}$ and $\ddot{\boldsymbol{u}}(t) = [\ddot{x}(t) \quad \ddot{y}(t)]^{\mathrm{T}}$. In addition, the body is subjected to two external forces, $f_x(t)$ and $f_y(t)$, acting in the x and y directions, respectively. To ensure analytical tractability and focus on the essential features of electromagnetic interaction, the following assumptions are adopted:

- The moving body is modeled as a particle.
- The springs are massless, linear, and exhibit no internal damping.
- Small displacements are assumed, so that geometric linearity is valid.
- Spring forces remain aligned with their respective directions.

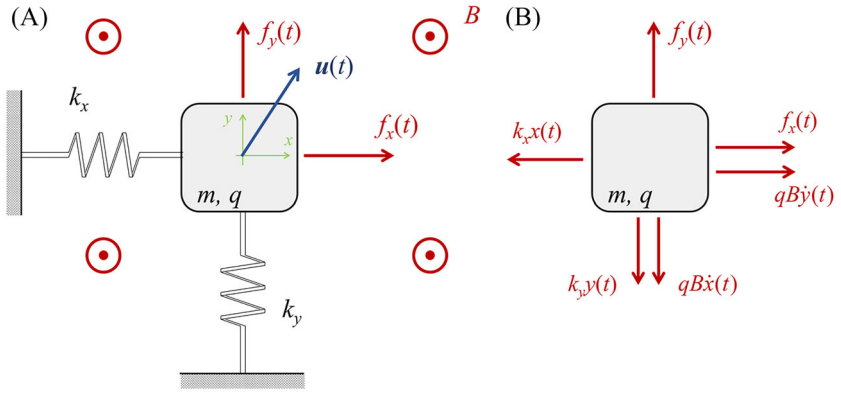

FIGURE 1 | Charged particle of mass m vibrating in a magnetic field with flux density B: (A) schematic of the model and (B) free-body diagram of the charged mass.

- Throughout the study, it is assumed that $k_x < k_y$.
- The magnetic flux density B is constant and uniform.
- Electromagnetic forces arise solely from velocity-dependent Lorentz interaction.

Figure 1B shows the free body diagram of the particle, indicating the external forces $f_x(t)$ and $f_y(t)$, the elastic restoring forces $k_x x(t)$ and $k_y y(t)$ from the springs, and the electromagnetic forces $qB\dot{x}(t)$ and $qB\dot{y}(t)$ arising from the interaction between the charge and the magnetic field. The latter are given by Lorentz law, $\boldsymbol{F}_{em} = q\dot{\boldsymbol{u}}(t) \wedge \boldsymbol{B}$. This results in a force component in the x-direction that depends on the velocity $\dot{y}(t)$ and another in the y-direction that depends on $\dot{x}(t)$. This means that the Lorentz force couples the motions $x(t)$ and $y(t)$ due to the interaction between the magnetic field $\boldsymbol{B}$ and the moving charge q. The equations of motion in the x and y directions then become

$$m\ddot{x}(t) - qB\dot{y}(t) + k_x x(t) = f_x(t), \tag{1}$$

$$m\ddot{y}(t) + qB\dot{x}(t) + k_y y(t) = f_y(t). \tag{2}$$

It can be noted that the coupling terms in these equations have opposite signs. This sign difference plays a crucial role in the dynamics of the system, as explored throughout the paper. These equations describe a two-degree-of-freedom system and can be expressed in matrix form as

$$\begin{bmatrix} m & 0 \\ 0 & m \end{bmatrix} \begin{Bmatrix} \ddot{x}(t) \\ \ddot{y}(t) \end{Bmatrix} + \begin{bmatrix} 0 & -qB \\ qB & 0 \end{bmatrix} \begin{Bmatrix} \dot{x}(t) \\ \dot{y}(t) \end{Bmatrix} + \begin{bmatrix} k_x & 0 \\ 0 & k_y \end{bmatrix} \begin{Bmatrix} x(t) \\ y(t) \end{Bmatrix} = \begin{Bmatrix} f_x(t) \\ f_y(t) \end{Bmatrix}, \tag{3}$$

which can be compactly written as

$$\boldsymbol{M}\ddot{\boldsymbol{u}}(t) + \boldsymbol{E}\dot{\boldsymbol{u}}(t) + \boldsymbol{K}\boldsymbol{u}(t) = \boldsymbol{f}(t), \tag{4}$$

where $\boldsymbol{M}$ is the mass matrix, $\boldsymbol{K}$ is the stiffness matrix, $\boldsymbol{E}$ represents the coupling matrix due to the Lorentz force, and $\boldsymbol{f}(t)$ is the external force vector. The mass and stiffness matrices are symmetric (actually, they are diagonal), while the coupling matrix is skew-symmetric, i.e., $\boldsymbol{E}^{\mathrm{T}} = -\boldsymbol{E}$.

Equation (4) resembles the second-order differential equation system typical of structural systems with viscous damping. However, in those cases, the damping matrix is usually symmetric with a dominant principal diagonal [30]. In contrast, here the skew-symmetric nature of the coupling matrix introduces distinctive dynamic properties. Some of these are reminiscent of gyroscopic systems, in which a skew-symmetric gyroscopic matrix couples the vibration modes of a rotating elastic body [31, 32]. Nevertheless, important differences arise, for example, with regard to stability, that are addressed in the following sections.

3 | Eigenvalue Problem

In this section, the eigenvalue problem of the system is solved and analyzed in depth. To examine the influence of the interaction between the charge and the magnetic field on mode coupling, the eigensolution of the uncoupled system is first presented. After, the eigenvalue problem of the coupled system is studied using both the configuration-space and the state-space formulations.

The configuration-space approach has the advantage of preserving the matrices of the original system. However, the orthogonality properties of the eigenvectors become more complex than those of conventional structural systems, as will be shown later. As a consequence, modal superposition cannot be applied in the conventional sense when solving for the system response.

In the state-space formulation, in turn, the number of degrees of freedom is doubled, which increases the size of the matrices and the computational cost. Nevertheless, in this case, the response of the state variables can be obtained through conventional modal superposition.

3.1 | Eigensolutions of the Uncoupled System

The particular case in the absence of a magnetic field, i.e., for $B = 0$, is now considered. In this case, the equations of motion are reduced to two uncoupled differential equations for the displacements $x(t)$ and $y(t)$, which can be expressed in matrix form as

$$\begin{bmatrix} m & 0 \\ 0 & m \end{bmatrix} \begin{Bmatrix} \ddot{x}(t) \\ \ddot{y}(t) \end{Bmatrix} + \begin{bmatrix} k_x & 0 \\ 0 & k_y \end{bmatrix} \begin{Bmatrix} x(t) \\ y(t) \end{Bmatrix} = \begin{Bmatrix} 0 \\ 0 \end{Bmatrix}. \tag{5}$$

The eigenvalues of this uncoupled two-degree-of-freedom system are given by $\omega_x = \sqrt{k_x/m}$ and $\omega_y = \sqrt{k_y/m}$. As previously stated, the condition $k_x \leq k_y$ is assumed, and therefore, $\omega_x \leq \omega_y$ holds. If $\omega_x \neq \omega_y$, the corresponding eigenvectors are $\boldsymbol{u}_x = [1 \quad 0]^{\mathrm{T}}$ and $\boldsymbol{u}_y = [0 \quad 1]^{\mathrm{T}}$, and the orthogonality property with respect to the mass and stiffness matrices is satisfied.

3.2 | Modal Properties in the Configuration Space

In this section, the modal properties of the system in configuration-space coordinates, defined by $x(t)$ and $y(t)$, are analyzed. The eigenvalues and eigenvectors are first examined in the general case. Then, the particular case of a coupled system derived from an uncoupled system exhibiting a double mode is considered. Finally, the orthogonality and normalization properties of the eigenvectors are addressed.

3.2.1 | Eigenvalues and Eigenvectors

Due to the structure of Equation (4), the eigensolution is fully defined by the eigenvalue problem with right eigenvectors $\boldsymbol{u}_{\mathrm{R}}$ and left eigenvectors $\boldsymbol{u}_{\mathrm{L}}$, derived, respectively, from

$$(-\omega^2\boldsymbol{M} + i\omega\boldsymbol{E} + \boldsymbol{K})\boldsymbol{u}_{\mathrm{R}} = \boldsymbol{0}, \tag{6}$$

$$\boldsymbol{u}_{\mathrm{L}}^{\mathrm{T}}(-\omega^2\boldsymbol{M} + i\omega\boldsymbol{E} + \boldsymbol{K}) = \boldsymbol{0}^{\mathrm{T}}. \tag{7}$$

Accordingly, the eigenvalues are obtained by solving the characteristic equation

$$\det(-\omega^2\boldsymbol{M} + i\omega\boldsymbol{E} + \boldsymbol{K}) = 0, \tag{8}$$

which yields a characteristic polynomial in ω. Two important conclusions can be drawn from the structure of Equations (6)–(8):

First, the transpose operator is applied to Equation (7), resulting in

$$(-\omega^2\boldsymbol{M} - i\omega\boldsymbol{E} + \boldsymbol{K})\boldsymbol{u}_{\mathrm{L}} = \boldsymbol{0}, \tag{9}$$

because $\boldsymbol{M}^{\mathrm{T}} = \boldsymbol{M}$, $\boldsymbol{K}^{\mathrm{T}} = \boldsymbol{K}$ and $\boldsymbol{E}^{\mathrm{T}} = -\boldsymbol{E}$. Therefore, the eigenvalues can equivalently be obtained from

$$\det(-\omega^2\boldsymbol{M} - i\omega\boldsymbol{E} + \boldsymbol{K}) = 0. \tag{10}$$

Since the characteristic equation must be unique, both Equations (8) and (10) must yield the same result. Hence, the characteristic equation can be expressed in terms of either $+\omega$ or $-\omega$, leading to the conclusion that it must contain only even powers of ω

$$(\omega_1^2 - \omega^2)(\omega_2^2 - \omega^2) = 0 \tag{11}$$

and, thus, the eigenvalues must be real and occur in pairs: $\pm\omega_1$ and $\pm\omega_2$. The positive values are associated with the right eigenvectors, while the negative values correspond to the left eigenvectors. This behavior contrasts with that of second-order systems with viscous damping, where the eigenvalues typically form complex conjugate pairs. The presence of real eigenvalues in the current system is consistent with the absence of damping.

Next, the Hermitian operator $(\cdot)^{\mathrm{H}}$ (i.e., the complex conjugate transpose) is applied to Equation (7), leading to

$$(-\omega^2\boldsymbol{M} + i\omega\boldsymbol{E} + \boldsymbol{K})\bar{\boldsymbol{u}}_{\mathrm{L}} = \boldsymbol{0}, \tag{12}$$

where $\overline{(\cdot)}$ denotes complex conjugation. The only imaginary term affected is $i\omega\boldsymbol{E}$, since the matrices are real and the eigenvalues were shown to be real. A comparison of Equations (6) and (12) reveals that they are in fact equivalent, which means that the right and left eigenvectors form complex conjugate pairs. This is another distinction from viscous systems with symmetric matrices, in which the complex right and left eigenvectors are identical.

In summary, due to the skew-symmetric nature of the electromagnetic coupling matrix $\boldsymbol{E}$, the eigenvalues of the coupled system are real and occur in opposite-sign pairs. The positive eigenvalues are associated with the right eigenvectors $\boldsymbol{u}_{\mathrm{R}}$, and the negative ones with the left eigenvectors $\boldsymbol{u}_{\mathrm{L}}$, which are their complex conjugates. From this point on, for notational simplicity, the right eigenvectors are denoted by $\boldsymbol{u}$ and the left ones by $\bar{\boldsymbol{u}}$.

Next, let us analyze the eigenvalues. The characteristic Equation (8) becomes

$$(\omega_x^2 - \omega^2)(\omega_y^2 - \omega^2) - C^2\omega^2 = 0, \tag{13}$$

where ω_x and ω_y are the natural angular frequencies of the uncoupled system, and the constant C is defined as

$$C = \frac{qB}{m}. \tag{14}$$

As expected, this is a second-order equation in ω^2. Before solving it, the functions $f_1(\omega^2)$ and $f_2(\omega^2)$, given by

$$f_1(\omega^2) = (\omega_x^2 - \omega^2)(\omega_y^2 - \omega^2), \tag{15}$$

$$f_2(\omega^2) = C^2\omega^2, \tag{16}$$

are plotted in Figure 2A.

In Figure 2A, the intersections between the blue parabola $f_1(\omega^2)$ and the abscissa axis correspond to the squared natural angular frequencies ω_x^2 and ω_y^2 of the uncoupled system, and the intersections between the blue parabola $f_1(\omega^2)$ and the red straight-line $f_2(\omega^2)$ yield the solutions of Equation (13), corresponding to ω_1^2 and ω_2^2, the squared natural angular frequencies of the coupled system due to the electromagnetic and mechanical interactions. Thus, the eigenvalues are again $\pm\omega_1$ and $\pm\omega_2$. From this figure, it can be deduced that the magnetic coupling causes a decrease in the lowest frequency and an increase in the highest one. These effects are directly related to the slope of $f_2(\omega^2)$, which is C^2: as this slope increases, ω_1 decreases and ω_2 increases. When the slope approaches verticality, it can be observed that the former tends to zero while the latter tends to infinity.

Specifically, by solving Equation (13), the resulting eigenvalues are given by

$$\omega_1^2 = \frac{\omega_x^2 + \omega_y^2 + C^2}{2} - \sqrt{\left(\frac{\omega_x^2 + \omega_y^2 + C^2}{2}\right)^2 - \omega_x^2\omega_y^2}, \tag{17}$$

$$\omega_2^2 = \frac{\omega_x^2 + \omega_y^2 + C^2}{2} + \sqrt{\left(\frac{\omega_x^2 + \omega_y^2 + C^2}{2}\right)^2 - \omega_x^2\omega_y^2}. \tag{18}$$

To illustrate the dependence on C, the values of ω_1 and ω_2 are represented in Figure 2B. In this figure, it can be observed that ω_1 asymptotically decreases toward zero, while ω_2 increases without bound, following the asymptote $\omega(C) = C$. This analysis of the eigenvalues confirms that all natural frequencies remain real and positive for any value of the coupling parameter. Consequently, the system exhibits bounded oscillatory motion and is unconditionally stable. This contrasts, for example, with gyroscopic systems involving a skew-symmetric matrix [31, 32], which can become unstable at specific rotational speeds (known as critical speeds).

Regarding the right eigenvectors, the solution of $\boldsymbol{u}_1$ and $\boldsymbol{u}_2$ corresponding to ω_1 and ω_2 are expressed as

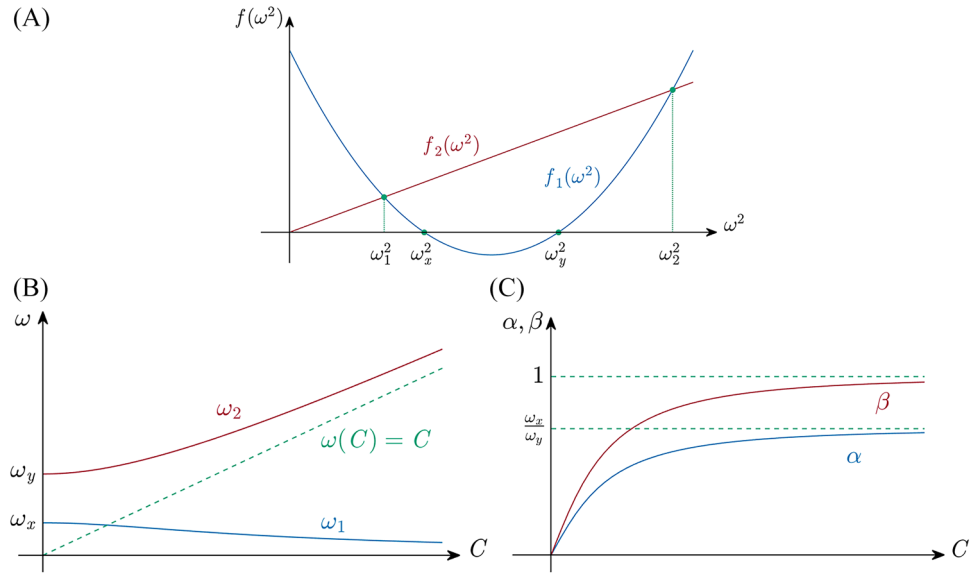

FIGURE 2 | Influence of the magnetic field on the modal properties of the system: (A) the intersection of the curves indicates that mode coupling leads to a decrease in the lowest natural frequency and an increase in the highest, relative to the uncoupled system; (B) evolution of the natural frequencies ω_1 and ω_2 of the coupled system as a function of the coupling parameter C and (C) evolution of the coefficients α and β of the eigenvectors of the coupled system as functions of the coupling parameter C.

$$\boldsymbol{u}_1 = \begin{Bmatrix} 1 \\ -\mathrm{i}\alpha \end{Bmatrix}, \boldsymbol{u}_2 = \begin{Bmatrix} -\mathrm{i}\beta \\ 1 \end{Bmatrix}, \tag{19}$$

where the coefficients α and β are real and positive, defined by

$$\alpha = \frac{\omega_x^2 - \omega_1^2}{C\omega_1}, \tag{20}$$

$$\beta = \frac{\omega_2^2 - \omega_y^2}{C\omega_2}, \tag{21}$$

respectively. These eigenvectors are presented without any particular normalization, to clearly exhibit the coupling terms introduced by the magnetic interaction. Normalization is addressed in Section 3.2.3. A comparison with the eigenvectors $\boldsymbol{u}_x$ and $\boldsymbol{u}_y$ of the uncoupled system reveals that the coupling between modes is introduced by purely imaginary terms. This leads to a phase difference between the motions $x(t)$ and $y(t)$, governed by the values of α and β. The dependence of these parameters on C is illustrated in Figure 2C. It should be noted that both α (blue line) and β (red line) are strictly increasing functions of C, indicating that the strength of mode coupling grows with the magnetic interaction. Furthermore, it is observed that $\beta > \alpha$; the former tends toward 1, while the latter approaches the ratio between the smallest and largest natural frequencies of the uncoupled system. This implies that the phase difference between the modal displacements tends to a constant as C increases.

3.2.2 | The Particular Case of the Double Mode

In this section, the particular case in which $k_x = k_y = k$ is analyzed. This condition implies that the uncoupled system possesses a double mode with a unique natural angular frequency, $\omega_0 = \sqrt{k/m}$, and no specific eigenvector can be defined. Under this condition, the characteristic Equation (13) for the coupled system becomes

$$(\omega_0^2 - \omega^2)^2 - C^2\omega^2 = 0. \tag{22}$$

As in the general case discussed previously, the new parabola $f_1(\omega^2)$ and straight-line $f_2(\omega^2)$ are represented in Figure 3A. The only intersection of the blue parabola $f_1(\omega^2)$ with the abscissa axis corresponds to the single-squared natural angular frequency of the uncoupled system ω_0^2. The intersections between the blue parabola and the red straight-line $f_2(\omega^2)$ illustrate how this frequency splits into two distinct values when the magnetic field is applied: a lower frequency ω_1^2 and a higher one ω_2^2. As in the general case, ω_1^2 decreases toward zero as the slope C^2 increases, while ω_2^2 increases without bound. Specifically, the resulting expressions for ω_1 and ω_2 are

$$\omega_1 = \sqrt{\omega_0^2 + \left(\frac{C}{2}\right)^2} - \frac{C}{2}, \tag{23}$$

$$\omega_2 = \sqrt{\omega_0^2 + \left(\frac{C}{2}\right)^2} + \frac{C}{2}. \tag{24}$$

Figure 3B shows the evolution of these angular frequencies as a function of the parameter C. The blue curve represents ω_1 and the red one ω_2. As previously described, it can be observed that the original natural frequency splits into two: one frequency decreases monotonically and asymptotically to zero, while the other increases without bound, following the asymptote $\omega(C) = C$.

Regarding the right eigenvectors, they are given by

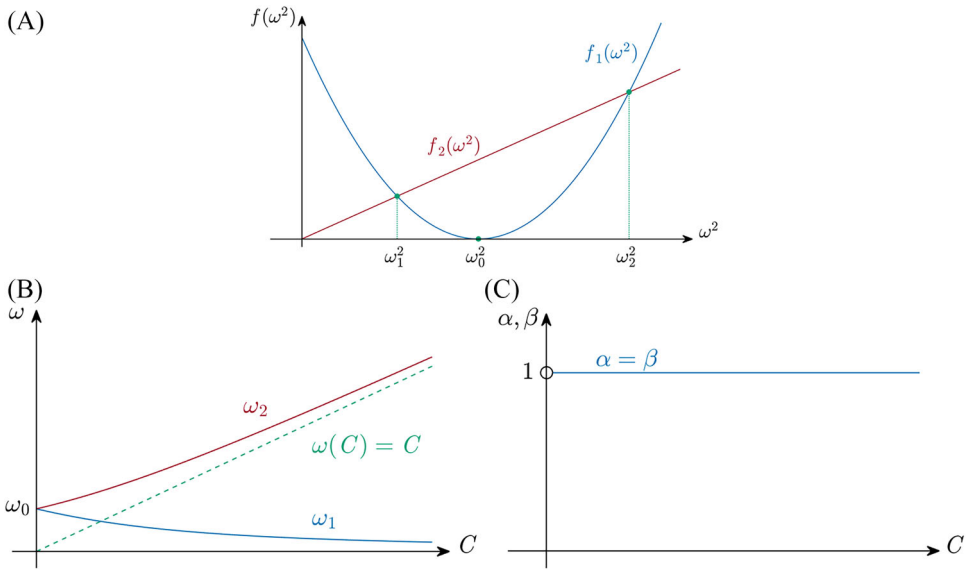

FIGURE 3 | Influence of the magnetic field on the modal properties of the coupled system when $k_x = k_y$: (A) the intersection of the curves indicates that mode coupling splits the double natural frequency ω_0 into two distinct frequencies: one lower (ω_1) and one higher (ω_2); (B) evolution of the natural frequencies ω_1 and ω_2 of the coupled system as a function of the coupling parameter C when $k_x = k_y$ and (C) evolution of the coefficients α and β of the eigenvectors of the coupled system as functions of the coupling parameter C.

$$\boldsymbol{u}_1 = \begin{Bmatrix} 1 \\ -\mathrm{i} \end{Bmatrix}, \ \boldsymbol{u}_2 = \begin{Bmatrix} -\mathrm{i} \\ 1 \end{Bmatrix}. \tag{25}$$

It can be noted that these eigenvectors remain constant. In other words, for the coupling in this case, the coefficients α and β are independent of the coupling constant C, as illustrated in Figure 3C. This figure shows that these coefficients take the fixed value $\alpha = \beta = 1$. This behavior represents a notable difference to the general case where $k_x \neq k_y$.

3.2.3 | Orthogonality and Normalization

The $\boldsymbol{M} - \boldsymbol{K}$ system without any mechanical-electrical-magnetic coupling given by Equation (5) is self-adjoint. Consequently, the eigenvectors are orthogonal with respect to the mass matrix $\boldsymbol{M}$ and the stiffness matrix $\boldsymbol{K}$. This property enables useful procedures related to normalization, diagonalization, and modal superposition.

However, for the coupled system, the self-adjoint property no longer holds, and the orthogonality relations become more complex than in the uncoupled case. To deduce these properties, the eigenvalue problem given by Equation (6) is considered for two distinct eigenvalues ω_i and ω_j,

$$\left(-\omega_i^2 \boldsymbol{M} + i\omega_i \boldsymbol{E} + \boldsymbol{K}\right)\boldsymbol{u}_i = \boldsymbol{0}, \tag{26}$$

$$\left(-\omega_j^2 \boldsymbol{M} + i\omega_j \boldsymbol{E} + \boldsymbol{K}\right)\boldsymbol{u}_j = \boldsymbol{0}. \tag{27}$$

The first equation is pre-multiplied by $\boldsymbol{u}_j^{\mathrm{T}}$ and the second by $\boldsymbol{u}_i^{\mathrm{T}}$, after which the second expression is transposed. These manipulations yield

$$\boldsymbol{u}_j^{\mathrm{T}}\left(-\omega_i^2 \boldsymbol{M} + i\omega_i \boldsymbol{E} + \boldsymbol{K}\right)\boldsymbol{u}_i = 0, \tag{28}$$

$$\boldsymbol{u}_j^{\mathrm{T}}\left(-\omega_j^2 \boldsymbol{M} - i\omega_j \boldsymbol{E} + \boldsymbol{K}\right)\boldsymbol{u}_i = 0. \tag{29}$$

By subtracting these two expressions, the following equation is obtained,

$$(\omega_i + \omega_j)\boldsymbol{u}_j^{\mathrm{T}}[(\omega_i - \omega_j)\boldsymbol{M} - i\boldsymbol{E}]\boldsymbol{u}_i = 0. \tag{30}$$

In addition, multiplying Equation (28) by ω_j and Equation (29) by ω_i, and adding the results leads to

$$(\omega_i + \omega_j)\boldsymbol{u}_j^{\mathrm{T}}(-\omega_i\omega_j \boldsymbol{M} + \boldsymbol{K})\boldsymbol{u}_i = 0. \tag{31}$$

From these, two orthogonality relations for the coupled system are derived,

$$\boldsymbol{u}_j^{\mathrm{T}}[(\omega_i - \omega_j)\boldsymbol{M} - i\boldsymbol{E}]\boldsymbol{u}_i = 0, \tag{32}$$

$$\boldsymbol{u}_j^{\mathrm{T}}(-\omega_i\omega_j \boldsymbol{M} + \boldsymbol{K})\boldsymbol{u}_i = 0. \tag{33}$$

For the case $i = j$, Equations (32) and (33) reduced to

$$\boldsymbol{u}_i^{\mathrm{T}} \boldsymbol{E} \boldsymbol{u}_i = 0, \tag{34}$$

$$\boldsymbol{u}_i^{\mathrm{T}}\left(-\omega_i^2 \boldsymbol{M} + \boldsymbol{K}\right)\boldsymbol{u}_i = 0. \tag{35}$$

Additional properties can be obtained by applying the Hermitian operator instead of the transpose. This results in

$$\boldsymbol{u}_j^{\mathrm{H}}\left(-\omega_i^2 \boldsymbol{M} + i\omega_i \boldsymbol{E} + \boldsymbol{K}\right)\boldsymbol{u}_i = 0, \tag{36}$$

$$\boldsymbol{u}_j^{\mathrm{H}}\left(-\omega_j^2\boldsymbol{M} + i\omega_j\boldsymbol{E} + \boldsymbol{K}\right)\boldsymbol{u}_i = 0. \tag{37}$$

Subtracting the two yields

$$(\omega_i - \omega_j)\boldsymbol{u}_j^{\mathrm{H}}[(\omega_i + \omega_j)\boldsymbol{M} - i\boldsymbol{E}]\boldsymbol{u}_i = 0. \tag{38}$$

Furthermore, by multiplying Equations (36) and (37) by ω_j and by ω_i, respectively, and subtracting, it follows that

$$(\omega_i - \omega_j)\boldsymbol{u}_j^{\mathrm{H}}[\omega_i\omega_j\boldsymbol{M} + \boldsymbol{K}]\boldsymbol{u}_i = 0. \tag{39}$$

Thus, for $i \neq j$, two additional orthogonality properties hold

$$\boldsymbol{u}_j^{\mathrm{H}}[(\omega_i + \omega_j)\boldsymbol{M} - i\boldsymbol{E}]\boldsymbol{u}_i = 0, \tag{40}$$

$$\boldsymbol{u}_j^{\mathrm{H}}[\omega_i\omega_j\boldsymbol{M} + \boldsymbol{K}]\boldsymbol{u}_i = 0. \tag{41}$$

As previously mentioned, the orthogonality relations in Equations (32)–(35), (40), and (41) are not as straightforward as in the uncoupled case, which limits their usefulness in diagonalization and modal superposition.

A final property can be derived for normalization. When $i = j$, Equations (38) and (39) become

$$\boldsymbol{u}_i^{\mathrm{H}}[2\omega_i\boldsymbol{M} - i\boldsymbol{E}]\boldsymbol{u}_i = \delta_i, \tag{42}$$

$$\boldsymbol{u}_i^{\mathrm{H}}\left[\omega_i^2\boldsymbol{M} + \boldsymbol{K}\right]\boldsymbol{u}_i = \gamma_i, \tag{43}$$

where the constants δ_i and γ_i satisfy the relation

$$\gamma_i = \omega_i\,\delta_i. \tag{44}$$

These expressions define a normalization method for the eigenvectors. For instance, the choice $\delta_i = 2\omega_i$ corresponds to the typical unit modal mass normalization of the uncoupled systems with $\boldsymbol{E} = \boldsymbol{0}$, similarly to systems with viscous damping [33].

3.3 | Modal Properties in the State Space

In this section, the modal properties derived from the state-space formulation are examined. The methods are similar to those used in classical problems involving viscous damping [30]. Therefore, a detailed development is not presented, but the key aspects are highlighted to enable the application of modal superposition in Sections 4 and 5, where the system response is obtained. First, the solution to the eigenvalue problem is outlined, followed by the orthogonality and normalization properties.

3.3.1 | Eigenvalues and Eigenvectors

The state vector $\boldsymbol{z}(t)$ associated with the displacement vector $\boldsymbol{u}(t)$ is defined as

$$\boldsymbol{z}(t) = \begin{Bmatrix}\boldsymbol{u}(t)\\ \boldsymbol{v}(t)\end{Bmatrix}, \tag{45}$$

where vector $\boldsymbol{v}(t)$ is referred to as the effective velocity, defined by the momentum equality

$$\boldsymbol{M}\boldsymbol{v}(t) = \boldsymbol{M}\dot{\boldsymbol{u}}(t). \tag{46}$$

With this definition, the generalized state-space form is written as

$$\boldsymbol{A}\dot{\boldsymbol{z}}(t) + \boldsymbol{B}\boldsymbol{z}(t) = \boldsymbol{0}, \tag{47}$$

where

$$\boldsymbol{A} = \begin{bmatrix}\boldsymbol{E} & \boldsymbol{M}\\ \boldsymbol{M} & \boldsymbol{0}\end{bmatrix}, \tag{48}$$

$$\boldsymbol{B} = \begin{bmatrix}\boldsymbol{K} & \boldsymbol{0}\\ \boldsymbol{0} & -\boldsymbol{M}\end{bmatrix}. \tag{49}$$

Matrix $\boldsymbol{B}$ is symmetric, whereas matrix $\boldsymbol{A}$ is neither symmetric nor skew-symmetric. The right and left eigenvalue problems are given by

$$(\mathrm{i}\omega\boldsymbol{A} + \boldsymbol{B})\boldsymbol{z}_{\mathrm{R}} = \boldsymbol{0}, \tag{50}$$

$$\boldsymbol{z}_{\mathrm{L}}^{\mathrm{T}}(\mathrm{i}\omega\boldsymbol{A} + \boldsymbol{B}) = \boldsymbol{0}^{\mathrm{T}}, \tag{51}$$

where $\boldsymbol{z}_{\mathrm{R}}$ and $\boldsymbol{z}_{\mathrm{L}}$ denote the right and left eigenvectors, respectively. The eigenvalues are obtained by solving the following determinant equation,

$$\det(\mathrm{i}\omega\boldsymbol{A} + \boldsymbol{B}) = 0. \tag{52}$$

The first property is derived by transposing Equation (51), which gives

$$(\mathrm{i}\omega\boldsymbol{A}^{\mathrm{T}} + \boldsymbol{B})\boldsymbol{z}_{\mathrm{L}} = \boldsymbol{0}. \tag{53}$$

This shows that the left eigenvectors of the original problem can be obtained as the right eigenvectors of the transposed problem, that is, the system defined by the matrices $\boldsymbol{A}^{\mathrm{T}}$ and $\boldsymbol{B}^{\mathrm{T}} = \boldsymbol{B}$.

To derive the second and third properties, Equation (50) is transposed, leading to

$$\boldsymbol{z}_{\mathrm{R}}^{\mathrm{T}}(\mathrm{i}\omega\boldsymbol{A}^{\mathrm{T}} + \boldsymbol{B}) = \boldsymbol{0}^{\mathrm{T}}, \tag{54}$$

and then the Hermite operator is applied,

$$(-\mathrm{i}\omega\boldsymbol{A} + \boldsymbol{B})\bar{\boldsymbol{z}}_{\mathrm{R}} = \boldsymbol{0}. \tag{55}$$

This result implies two things: first, the right eigenvectors form complex conjugate pairs (and a similar result holds for the left eigenvectors); second, the eigenvalues can also be obtained from

$$\det(-\mathrm{i}\omega \boldsymbol{A} + \boldsymbol{B}) = 0. \tag{56}$$

Therefore, it is concluded that, as in the configuration-space formulation, the eigenvalues are real and appear in positive and negative pairs. Specifically, the four eigenvalues are ω_1, ω_2, $-\omega_1$ and $-\omega_2$, as given in Equations (17) and (18). The corresponding right eigenvectors are

$$\boldsymbol{z}_{\mathrm{R},1} = \begin{Bmatrix} 1 \\ -\mathrm{i}\alpha \\ \mathrm{i}\omega_1 \\ \omega_1\alpha \end{Bmatrix}, \boldsymbol{z}_{\mathrm{R},2} = \begin{Bmatrix} -\mathrm{i}\beta \\ 1 \\ \omega_2\beta \\ \mathrm{i}\omega_2 \end{Bmatrix}, \boldsymbol{z}_{\mathrm{R},3} = \bar{\boldsymbol{z}}_{\mathrm{R},1}, \boldsymbol{z}_{\mathrm{R},4} = \bar{\boldsymbol{z}}_{\mathrm{R},2}. \tag{57}$$

An important property can be deduced from this expression: the components corresponding to the coordinates $x(t)$ and $y(t)$, i.e., the first two components, match the eigenvectors of the configuration space, as given in Equation (19). In other words, Equation (57) can be alternatively written as

$$\boldsymbol{z}_{\mathrm{R},1} = \begin{Bmatrix} \boldsymbol{u}_1 \\ \mathrm{i}\omega_1\boldsymbol{u}_1 \end{Bmatrix}, \boldsymbol{z}_{\mathrm{R},2} = \begin{Bmatrix} \boldsymbol{u}_2 \\ \mathrm{i}\omega_2\boldsymbol{u}_2 \end{Bmatrix}, \boldsymbol{z}_{\mathrm{R},3} = \bar{\boldsymbol{z}}_{\mathrm{R},1}, \boldsymbol{z}_{\mathrm{R},4} = \bar{\boldsymbol{z}}_{\mathrm{R},2}. \tag{58}$$

Regarding the left eigenvectors, they result in

$$\boldsymbol{z}_{\mathrm{L},1} = \begin{Bmatrix} 1 \\ \mathrm{i}\alpha \\ \mathrm{i}\omega_1 \\ -\omega_1\alpha \end{Bmatrix}, \boldsymbol{z}_{\mathrm{L},2} = \begin{Bmatrix} \mathrm{i}\beta \\ 1 \\ -\omega_2\beta \\ \mathrm{i}\omega_2 \end{Bmatrix}, \boldsymbol{z}_{\mathrm{L},3} = \bar{\boldsymbol{z}}_{\mathrm{L},1}, \boldsymbol{z}_{\mathrm{L},4} = \bar{\boldsymbol{z}}_{\mathrm{L},2}, \tag{59}$$

which leads to the conclusion that they can be obtained from the complex conjugates of the right eigenvectors in the configuration space, as follows:

$$\boldsymbol{z}_{\mathrm{L},1} = \begin{Bmatrix} \bar{\boldsymbol{u}}_1 \\ \mathrm{i}\omega_1\bar{\boldsymbol{u}}_1 \end{Bmatrix}, \boldsymbol{z}_{\mathrm{L},2} = \begin{Bmatrix} \bar{\boldsymbol{u}}_2 \\ \mathrm{i}\omega_2\bar{\boldsymbol{u}}_2 \end{Bmatrix}, \boldsymbol{z}_{\mathrm{L},3} = \bar{\boldsymbol{z}}_{\mathrm{L},1}, \boldsymbol{z}_{\mathrm{L},4} = \bar{\boldsymbol{z}}_{\mathrm{L},2}. \tag{60}$$

3.3.2 | Orthogonality and Normalization

The orthogonality relations for the state-space formulation are derived using the right and left eigenvectors defined previously, following a structure similar to that used in classical systems with viscous damping [30]. They are succinctly revised next.

Let $\boldsymbol{z}_{\mathrm{R},i}$ and $\boldsymbol{z}_{\mathrm{L},j}$ be the right and left eigenvectors associated with the eigenvalues ω_i and ω_j, respectively, $\omega_i \neq \omega_j$. These vectors satisfy

$$(\mathrm{i}\omega_i\boldsymbol{A} + \boldsymbol{B})\boldsymbol{z}_{\mathrm{R},i} = \boldsymbol{0}, \tag{61}$$

$$\boldsymbol{z}_{\mathrm{L},j}^{\mathrm{T}}(\mathrm{i}\omega_j\boldsymbol{A} + \boldsymbol{B}) = \boldsymbol{0}^{\mathrm{T}}. \tag{62}$$

To derive orthogonality relations, Equation (61) is pre-multiplied by $\mathbf{z}_{\mathrm{L},j}^{\mathrm{T}}$ and Equation (62) is multiplied by $\mathbf{z}_{\mathrm{R},i}$. These manipulations led to the following two relations,

$$\boldsymbol{z}_{\mathrm{L},j}^{\mathrm{T}}(\mathrm{i}\omega_i\boldsymbol{A} + \boldsymbol{B})\boldsymbol{z}_{\mathrm{R},i} = 0, \tag{63}$$

$$\boldsymbol{z}_{\mathrm{L},j}^{\mathrm{T}}(\mathrm{i}\omega_j\boldsymbol{A} + \boldsymbol{B})\boldsymbol{z}_{\mathrm{R},i} = 0. \tag{64}$$

By subtracting these two equations, the orthogonality relation

$$\boldsymbol{z}_{\mathrm{L},j}^{\mathrm{T}}\boldsymbol{A}\boldsymbol{z}_{\mathrm{R},i} = 0 \tag{65}$$

is obtained. Likewise, multiplying Equations (63) and (64) by ω_j and ω_i, respectively, and subtracting them yields

$$\boldsymbol{z}_{\mathrm{L},j}^{\mathrm{T}}\boldsymbol{B}\boldsymbol{z}_{\mathrm{R},i} = 0. \tag{66}$$

These results indicate that the eigenvectors associated with different eigenvalues are orthogonal with respect to both matrices $\boldsymbol{A}$ and $\boldsymbol{B}$.

For the case $i = j$, the relations become self-inner products. The expressions

$$\boldsymbol{z}_{\mathrm{L},i}^{\mathrm{T}}\boldsymbol{A}\boldsymbol{z}_{\mathrm{R},i} = \phi_i, \tag{67}$$

$$\boldsymbol{z}_{\mathrm{L},i}^{\mathrm{T}}\boldsymbol{B}\boldsymbol{z}_{\mathrm{R},i} = \varphi_i, \tag{68}$$

define two constants, ϕ_i and φ_i, which characterize the normalization of the eigenvectors. It can be verified that these constants satisfy the identity

$$\varphi_i = -\mathrm{i}\omega_i\phi_i. \tag{69}$$

This relation mirrors the one derived in the configuration-space formulation and can be used as a basis for normalization. In particular, the eigenvectors can be normalized so that

$$\phi_i = 1 \rightarrow \varphi_i = -\mathrm{i}\omega_i. \tag{70}$$

This choice is consistent with the standard normalization applied to modal vectors in undamped systems and allows for direct application of modal superposition in the analysis of the system response.

4 | Free Vibration

The free vibration response of the charged mass under initial conditions can be obtained by several approaches: direct integration methods such as the Newmark method, direct method in the configuration space, or modal superposition in the state space.

Direct integration is straightforward, since it does not require prior computation of the eigenvalues and eigenvectors; however, it provides no insight into the modal contributions of the system. In contrast, modal superposition in the state space yields information about the participation of each mode. This method, however, presents two drawbacks: the dimensionality of the matrices is doubled, increasing computational demands,

and the resulting eigenvectors do not correspond to those of the configuration space, representing "fictitious" modes instead.

On the other hand, the response in the configuration space enables the study of the actual modes of the system, although classical modal superposition via diagonalization cannot be applied.

4.1 | Response in the Configuration Space

The response $\boldsymbol{u}(t)$ of the charged mass can be expressed by the contribution of the eigenmodes. As previously established, the system possesses four eigenpairs: two real eigenvalue pairs $\pm\omega_i$ and the associated complex conjugate eigenvectors $\boldsymbol{u}_i$ and $\bar{\boldsymbol{u}}_i$. Accordingly, the position $\boldsymbol{u}(t)$ and velocity $\dot{\boldsymbol{u}}(t)$ of the charged mass are given by

$$\boldsymbol{u}(t) = \sum_{i=1}^{n} \left(A_i \boldsymbol{u}_i e^{i\omega_i t} + B_i \bar{\boldsymbol{u}}_i e^{-i\omega_i t} \right), \tag{71}$$

$$\dot{\boldsymbol{u}}(t) = \sum_{i=1}^{n} i\omega_i \left(A_i \boldsymbol{u}_i e^{i\omega_i t} - B_i \bar{\boldsymbol{u}}_i e^{-i\omega_i t} \right), \tag{72}$$

respectively, where A_i and B_i are coefficients determined by the initial conditions $\boldsymbol{u}_0$ and $\dot{\boldsymbol{u}}_0$. Although in the present study $n = 2$, the subsequent formulation is presented in a general form valid for any number of degrees of freedom n.

The coefficients A_i and B_i are complex, yielding a total of $2n$ unknowns (one pair per eigenmode). These coefficients are related to the initial conditions as follows:

$$\boldsymbol{u}_0 = \sum_{i=1}^{n} (A_i \boldsymbol{u}_i + B_i \bar{\boldsymbol{u}}_i), \tag{73}$$

$$\dot{\boldsymbol{u}}_0 = \sum_{i=1}^{n} i\omega_i (A_i \boldsymbol{u}_i - B_i \bar{\boldsymbol{u}}_i). \tag{74}$$

Considering that the initial conditions are purely real, it follows that the pairs A_i and B_i must be complex conjugates. To show this, the eigenvectors $\boldsymbol{u}_i$ are decomposed into their real and imaginary components, denoted as $\boldsymbol{v}_i$ and $\boldsymbol{w}_i$, respectively:

$$\boldsymbol{u}_i = \boldsymbol{v}_i + i\boldsymbol{w}_i. \tag{75}$$

Substituting this decomposition into the expressions for $\boldsymbol{u}_0$ and $\dot{\boldsymbol{u}}_0$ yields

$$\boldsymbol{u}_0 = \sum_{i=1}^{n} [A_i(\boldsymbol{v}_i + i\boldsymbol{w}_i) + B_i(\boldsymbol{v}_i - i\boldsymbol{w}_i)], \tag{76}$$

$$\dot{\boldsymbol{u}}_0 = \sum_{i=1}^{n} i\omega_i [A_i(\boldsymbol{v}_i + i\boldsymbol{w}_i) - B_i(\boldsymbol{v}_i - i\boldsymbol{w}_i)]. \tag{77}$$

These expressions must yield real vectors. Thus, their imaginary parts must vanish:

$$\mathrm{Im}[\boldsymbol{v}_i(A_i + B_i) + i\boldsymbol{w}_i(A_i - B_i)] = \boldsymbol{0}, \tag{78}$$

$$\mathrm{Im}[-\omega_i \boldsymbol{w}_i(A_i + B_i) + i\omega_i \boldsymbol{v}_i(A_i - B_i)] = \boldsymbol{0}. \tag{79}$$

These conditions are satisfied if A_i and B_i are complex conjugates,

$$B_i = \bar{A}_i. \tag{80}$$

Therefore, these coefficients can be expressed as complex numbers as

$$A_i = a_i + ib_i, \tag{81}$$

$$\bar{A}_i = a_i - ib_i, \tag{82}$$

and the initial conditions become

$$\boldsymbol{u}_0 = 2\sum_{i=1}^{n} (a_i \boldsymbol{v}_i - b_i \boldsymbol{w}_i), \tag{83}$$

$$\dot{\boldsymbol{u}}_0 = -2\sum_{i=1}^{n} \omega_i (a_i \boldsymbol{w}_i + b_i \boldsymbol{v}_i). \tag{84}$$

To solve for the coefficients a_i and b_i, the matrices $\boldsymbol{V}$, $\boldsymbol{W}$, and $\boldsymbol{\Omega}$ are introduced as

$$\boldsymbol{V} = [\boldsymbol{v}_1 \quad \boldsymbol{v}_2 \quad \cdots \quad \boldsymbol{v}_n], \tag{85}$$

$$\boldsymbol{W} = [\boldsymbol{w}_1 \quad \boldsymbol{w}_2 \quad \cdots \quad \boldsymbol{w}_n], \tag{86}$$

$$\boldsymbol{\Omega} = [\mathrm{diag}(\omega_i)]. \tag{87}$$

The coefficients a_i and b_i are grouped into the following column vectors:

$$\boldsymbol{a} = [a_1 \quad a_2 \quad \cdots \quad a_n]^{\mathrm{T}}, \tag{88}$$

$$\boldsymbol{b} = [b_1 \quad b_2 \quad \cdots \quad b_n]^{\mathrm{T}}. \tag{89}$$

The system of initial conditions can then be recast in matrix form as

$$\boldsymbol{u}_0 = 2(\boldsymbol{V}\boldsymbol{a} - \boldsymbol{W}\boldsymbol{b}), \tag{90}$$

$$\dot{\boldsymbol{u}}_0 = -2\boldsymbol{\Omega}(\boldsymbol{W}\boldsymbol{a} + \boldsymbol{V}\boldsymbol{b}). \tag{91}$$

Solving for $\boldsymbol{a}$ and $\boldsymbol{b}$ gives

$$\boldsymbol{a} = \frac{1}{2}(\boldsymbol{V} + \boldsymbol{W}\boldsymbol{\Omega}^{-1}\boldsymbol{V}^{-1}\boldsymbol{W}\boldsymbol{\Omega})^{-1}(\boldsymbol{u}_0 - \boldsymbol{W}\boldsymbol{\Omega}^{-1}\boldsymbol{V}^{-1}\dot{\boldsymbol{u}}_0), \tag{92}$$

$$\boldsymbol{b} = -\frac{1}{2}(\boldsymbol{W} + \boldsymbol{V}\boldsymbol{\Omega}^{-1}\boldsymbol{W}^{-1}\boldsymbol{V}\boldsymbol{\Omega})^{-1}(\boldsymbol{u}_0 + \boldsymbol{V}\boldsymbol{\Omega}^{-1}\boldsymbol{W}^{-1}\dot{\boldsymbol{u}}_0). \tag{93}$$

It should be noted that, in this study, the system has only two degrees of freedom, making the matrix inversion straightforward. Nonetheless, in more general cases with a larger number of degrees of freedom, solving the system numerically may be

more efficient. In such cases, the following linear system can be used:

$$\begin{bmatrix} \boldsymbol{V} & -\boldsymbol{W} \\ -\boldsymbol{\Omega W} & -\boldsymbol{\Omega V} \end{bmatrix} \begin{Bmatrix} \boldsymbol{a} \\ \boldsymbol{b} \end{Bmatrix} = \frac{1}{2} \begin{Bmatrix} \boldsymbol{u}_0 \\ \dot{\boldsymbol{u}}_0 \end{Bmatrix}. \tag{94}$$

In either case, the response $\boldsymbol{u}(t)$ is finally given by

$$\begin{aligned} \boldsymbol{u}(t) = 2\boldsymbol{V}(\cos\,\boldsymbol{\Omega}t\;\;\boldsymbol{a} - \;\sin\,\boldsymbol{\Omega}t\;\;\boldsymbol{b}) \\ - 2\boldsymbol{W}(\cos\,\boldsymbol{\Omega}t\;\;\boldsymbol{b} + \;\sin\,\boldsymbol{\Omega}t\;\;\boldsymbol{a}), \end{aligned} \tag{95}$$

where cos $\boldsymbol{\Omega}t$ and sin $\boldsymbol{\Omega}t$ denote diagonal matrices with entries cos $\omega_i t$ and sin $\omega_i t$, respectively. This equation represents a superposition of undamped vibrations with angular frequencies ω_i. However, it does not correspond to a conventional mode superposition, since the system is not self-adjoint. As a result, the motion described by Equation (95) cannot be interpreted as a sum of independent modal contributions. This behavior is illustrated in the numerical example presented in Section 6.

4.2 | Modal Superposition in the State Space

The advantage of studying the free response through the state-space formulation is that the response can be obtained by classical mode superposition. This means that the state variable $\boldsymbol{z}(t)$ can be obtained as the result of the contribution of each eigenvector $\boldsymbol{z}_{\mathrm{R},i}$ whose participation is given by the modal coordinate $q_i(t)$. Then, the state variable can be written as

$$\boldsymbol{z}(t) = \boldsymbol{Z}_{\mathrm{R}}\boldsymbol{q}(t), \tag{96}$$

where $\boldsymbol{Z}_{\mathrm{R}}$ is the matrix of the right eigenvectors arranged in columns,

$$\boldsymbol{Z}_{\mathrm{R}} = [\boldsymbol{z}_{\mathrm{R},1} \quad \boldsymbol{z}_{\mathrm{R},2} \quad \cdots \quad \boldsymbol{z}_{\mathrm{R},2n}], \tag{97}$$

and $\boldsymbol{q}(t)$ is the column vector of the modal coordinates,

$$\boldsymbol{q}(t) = [q_1(t) \quad q_2(t) \quad \cdots \quad q_{2n}(t)]^{\mathrm{T}}. \tag{98}$$

Then, Equation (47) can be written as

$$\boldsymbol{A}\boldsymbol{Z}_{\mathrm{R}}\dot{\boldsymbol{q}}(t) + \boldsymbol{B}\boldsymbol{Z}_{\mathrm{R}}\boldsymbol{q}(t) = \boldsymbol{0}, \tag{99}$$

which can be pre-multiplied by $\boldsymbol{Z}_{\mathrm{L}}^{\mathrm{T}}$, where $\boldsymbol{Z}_{\mathrm{L}}$ is the matrix of the left eigenvectors arranged in columns,

$$\boldsymbol{Z}_{\mathrm{L}} = [\boldsymbol{z}_{\mathrm{L},1} \quad \boldsymbol{z}_{\mathrm{L},2} \quad \cdots \quad \boldsymbol{z}_{\mathrm{L},2n}], \tag{100}$$

yielding

$$\boldsymbol{Z}_{\mathrm{L}}^{\mathrm{T}}\boldsymbol{A}\boldsymbol{Z}_{\mathrm{R}}\dot{\boldsymbol{q}}(t) + \boldsymbol{Z}_{\mathrm{L}}^{\mathrm{T}}\boldsymbol{B}\boldsymbol{Z}_{\mathrm{R}}\boldsymbol{q}(t) = \boldsymbol{0}. \tag{101}$$

Taking into account the orthogonality properties of the eigenvectors deduced in the previous section, it can be deduced that the system equations (101) can be decoupled for the $2n$ modal coordinates $q_i(t)$. The differential equation for the modal coordinates results in

$$\phi_i\dot{q}_i(t) + \varphi_i q_i(t) = 0, \tag{102}$$

where by considering the relation between ϕ_i and φ_i given by Equation (69), $\varphi_i = -\mathrm{i}\omega_i\phi_i$, the solution for the modal coordinates yields

$$q_i(t) = Q_i\mathrm{e}^{-\mathrm{i}\omega_i t}. \tag{103}$$

This equation represents harmonic functions with amplitudes Q_i, which depend on the initial conditions $\boldsymbol{z}_0$ of the state variable, given by

$$\boldsymbol{z}_0 = \begin{Bmatrix} \boldsymbol{u}_0 \\ \dot{\boldsymbol{u}}_0 \end{Bmatrix}. \tag{104}$$

The amplitude vector $\boldsymbol{Q}$, defined as

$$\boldsymbol{Q} = [Q_1 \quad Q_2 \quad \cdots \quad Q_{2n}]^{\mathrm{T}}, \tag{105}$$

can be obtained from the initial value of Equation (96),

$$\boldsymbol{z}_0 = \boldsymbol{Z}_{\mathrm{R}}\boldsymbol{Q}. \tag{106}$$

To avoid inverting matrix $\boldsymbol{Z}_{\mathrm{R}}$, Equation (106) can be multiplied to the left by matrix $\boldsymbol{Z}_{\mathrm{L}}^{\mathrm{T}}\boldsymbol{A}$,

$$\boldsymbol{Z}_{\mathrm{L}}^{\mathrm{T}}\boldsymbol{A}\boldsymbol{z}_0 = \boldsymbol{Z}_{\mathrm{L}}^{\mathrm{T}}\boldsymbol{A}\boldsymbol{Z}_{\mathrm{R}}\boldsymbol{Q}, \tag{107}$$

because matrix $\boldsymbol{Z}_{\mathrm{L}}^{\mathrm{T}}\boldsymbol{A}\boldsymbol{Z}_{\mathrm{R}}$ that multiplies $\boldsymbol{Q}$ is diagonal, and its inverse is straightforward. Moreover, if the eigenvectors are normalized as proposed by Equation (70), that matrix becomes the identity matrix, and the amplitude vector yields

$$\boldsymbol{Q} = \boldsymbol{Z}_{\mathrm{L}}^{\mathrm{T}}\boldsymbol{A}\boldsymbol{z}_0. \tag{108}$$

Finally, the response of the state vector $\boldsymbol{z}(t)$ results in the superposition of harmonic motions in which each eigenvector is multiplied by the modal contribution factor Q_i,

$$\boldsymbol{z}(t) = \boldsymbol{Z}_{\mathrm{R}}[\mathrm{diag}(\boldsymbol{q}(t))] = \sum_{i=1}^{2n} \boldsymbol{z}_{\mathrm{R},i}Q_i\mathrm{e}^{-\mathrm{i}\omega_i t}. \tag{109}$$

To conclude, two of the properties derived in the previous section must be considered: the eigenvalues appear in pairs with $\pm$ signs and the eigenvectors are complex conjugate pairs. Then, the previous equation can be rewritten as

$$\boldsymbol{z}(t) = \sum_{i=1}^{n} \left(\boldsymbol{z}_{\mathrm{R},i}Q_i\mathrm{e}^{-\mathrm{i}\omega_i t} + \overline{\boldsymbol{z}_{\mathrm{R},i}Q_i}\mathrm{e}^{\mathrm{i}\omega_i t}\right), \tag{110}$$

which can be simplified as

$$\boldsymbol{z}(t) = \sum_{i=1}^{n} (\mathrm{Re}(\boldsymbol{z}_{\mathrm{R},i} Q_i)\cos\ \omega_i t + \mathrm{Im}(\boldsymbol{z}_{\mathrm{R},i} Q_i)\sin\ \omega_i t). \quad (111)$$

Finally, the solution for the original variable $\boldsymbol{u}(t)$ can be obtained as

$$\boldsymbol{u}(t) = \sum_{i=1}^{n} (\mathrm{Re}(\boldsymbol{u}_i Q_i)\cos\ \omega_i t + \mathrm{Im}(\boldsymbol{u}_i Q_i)\sin\ \omega_i t), \quad (112)$$

which gives the same response as the one obtained in the configuration space, Equation (95).

5 | Frequency Response

In this section, the frequency response is obtained by assuming that the two external forces $f_x(t)$ and $f_y(t)$ actuating on the charged mass are harmonic share the same excitation angular frequency ω and are in phase. Then, the force vector is given by

$$\boldsymbol{f}(t) = \boldsymbol{F}\mathrm{e}^{\mathrm{i}\omega t}, \quad (113)$$

where $\boldsymbol{F} = [F_x \quad F_y]^{\mathrm{T}}$ is the force amplitude vector, with F_x and F_y denoting the components in the x and y directions, respectively. First, the response in the configuration space is described, followed by the response in the state space.

5.1 | Frequency Response in the Configuration Space

The orthogonality properties developed in Section 4.1 are not straightforward and do not allow the response to be obtained by modal superposition. For this reason, the harmonic response can only be computed directly from the Fourier transform of Equation (4), given by

$$(-\omega^2\boldsymbol{M} + i\omega\boldsymbol{E} + \boldsymbol{K})\boldsymbol{U}(\omega) = \boldsymbol{F}, \quad (114)$$

where $\boldsymbol{U}(\omega) = [U_x(\omega) \quad U_y(\omega)]^{\mathrm{T}}$ is the complex displacement amplitude vector depending on ω, and $U_x(\omega)$ and $U_y(\omega)$ are its components. In a system with only two degrees of freedom, as those studied in this paper, the vector $\boldsymbol{U}(\omega)$ can be easily computed by inverting the dynamic stiffness matrix at each angular frequency ω,

$$\boldsymbol{U}(\omega) = (-\omega^2\boldsymbol{M} + i\omega\boldsymbol{E} + \boldsymbol{K})^{-1}\boldsymbol{F}. \quad (115)$$

However, in a general case involving a larger number of degrees of freedom, matrix inversion is not recommended, and numerical methods such as decomposition algorithms are more suitable. For the specific system analyzed in this paper, the displacement amplitudes can be computed exactly, yielding

$$U_x(\omega) = \frac{(\omega_y^2 - \omega^2)F_x + \mathrm{i}\omega C F_y}{m(\omega_1^2 - \omega^2)(\omega_2^2 - \omega^2)}, \quad (116)$$

$$U_y(\omega) = \frac{(\omega_x^2 - \omega^2)F_y - \mathrm{i}\omega C F_x}{m(\omega_1^2 - \omega^2)(\omega_2^2 - \omega^2)}. \quad (117)$$

These displacement amplitudes are complex, indicating a phase difference between the displacements $x(t)$ and $y(t)$, and the applied forces. Specifically, the imaginary terms appear in the cross terms, i.e., in the relation between the amplitude $U_x(\omega)$ and the force F_y, and between the amplitude $U_y(\omega)$ and the force F_x. These relations are better illustrated using the frequency response functions (FRFs) $H_{jk}(\omega)$, which represent the ratio between the displacement amplitude associated with the j-th degree of freedom and the force associated with the k-th one. The four FRFs of this system are given by

$$H_{xx}(\omega) = \frac{U_x(\omega)}{F_x} = \frac{\omega_y^2 - \omega^2}{m(\omega_1^2 - \omega^2)(\omega_2^2 - \omega^2)}, \quad (118)$$

$$H_{xy}(\omega) = \frac{U_x(\omega)}{F_y} = \frac{\mathrm{i}\omega C}{m(\omega_1^2 - \omega^2)(\omega_2^2 - \omega^2)}, \quad (119)$$

$$H_{yx}(\omega) = \frac{U_y(\omega)}{F_x} = \frac{-\mathrm{i}\omega C}{m(\omega_1^2 - \omega^2)(\omega_2^2 - \omega^2)}, \quad (120)$$

$$H_{yy}(\omega) = \frac{U_y(\omega)}{F_y} = \frac{\omega_x^2 - \omega^2}{m(\omega_1^2 - \omega^2)(\omega_2^2 - \omega^2)}. \quad (121)$$

These FRFs constitute the receptance matrix $\boldsymbol{H}(\omega)$, which satisfies

$$\boldsymbol{U}(\omega) = \boldsymbol{H}(\omega)\boldsymbol{F}. \quad (122)$$

The receptance matrix represents the frequency response model of the system. As previously noted, the direct FRFs $H_{xx}(\omega)$ and $H_{yy}(\omega)$, corresponding to the principal diagonal, are real, while the cross FRFs $H_{xy}(\omega)$ and $H_{yx}(\omega)$ are purely imaginary. Furthermore, the cross FRFs have equal magnitude but opposite signs, i.e., $H_{yx}(\omega) = -H_{xy}(\omega)$. Therefore, Maxwell's reciprocity principle is not satisfied, suggesting that there exists energy transfer between modes. This differs from systems with viscous damping, in which both the direct and cross FRFs are complex, and the cross FRFs share both magnitude and sign. In such systems, the receptance matrix is symmetric because the damping matrix is also symmetric [30], whereas in the present system, due to the mechanical-electrical-magnetic coupling matrix $\boldsymbol{E}$, the damping matrix is not symmetric.

To conclude this section, the following properties are stated, which can also be deduced from the displacement amplitude expressions (116) and (117):

Although Equation (114) has a form similar to that of systems with viscous damping, the skew-symmetric nature of the coupling matrix $\boldsymbol{E}$ implies that the system is undamped, as the associated one performs no work. Therefore, the resonance frequencies coincide with the natural frequencies studied in Section 3.2.1, and the response tends to infinity at resonance.

In the absence of a magnetic field, i.e., for $C = 0$, the response amplitudes correspond to the uncoupled case,

$$U_x(\omega) = \frac{F_x}{m(\omega_x^2 - \omega^2)}, U_y(\omega) = \frac{F_y}{m(\omega_y^2 - \omega^2)}. \quad (123)$$

In both the uncoupled and the coupled cases, when the excitation frequency tends to zero, $\omega \to 0$, the amplitudes correspond to the static case,

$$U_x = \frac{F_x}{k_x}, U_y = \frac{F_y}{k_y}. \quad (124)$$

When the excitation frequency tends to infinity, $\omega \to \infty$, the displacement amplitudes tend to zero.

5.2 | Frequency Response in the State Space

The equation in the state space of the system subjected to the harmonic force is

$$\boldsymbol{A}\dot{\boldsymbol{z}}(t) + \boldsymbol{B}\boldsymbol{z}(t) = \hat{\boldsymbol{f}}(t), \quad (125)$$

where

$$\hat{\boldsymbol{f}}(t) = \begin{Bmatrix} \boldsymbol{f}(t) \\ \boldsymbol{0} \end{Bmatrix}. \quad (126)$$

The zero vector in this equation has the same length as $\boldsymbol{f}(t)$. The harmonic response is obtained from the Fourier transform of Equation (125),

$$(i\omega\boldsymbol{A} + \boldsymbol{B})\boldsymbol{Z}(\omega) = \hat{\boldsymbol{F}}, \quad (127)$$

where $\hat{\boldsymbol{F}}$ represents the amplitude vector of the state forces, and $\boldsymbol{Z}(\omega)$ is the complex amplitude vector of the state variables depending on ω. The main advantage of this formulation is that, due to the orthogonality properties, the response can be obtained by modal superposition. To this end, the same procedure as in the free vibration analysis must be followed. That is, the change of variables to modal coordinates, as Equation (96), must be applied,

$$(i\omega\boldsymbol{A} + \boldsymbol{B})\boldsymbol{Z}_R\boldsymbol{Q}(\omega) = \hat{\boldsymbol{F}}, \quad (128)$$

where $\boldsymbol{Q}(\omega)$ is the modal contribution vector depending on ω. This equation is then multiplied on the left by the transpose of the left eigenvector matrix $\boldsymbol{Z}_L^T$,

$$\boldsymbol{Z}_L^T(i\omega\boldsymbol{A} + \boldsymbol{B})\boldsymbol{Z}_R\boldsymbol{Q}(\omega) = \boldsymbol{Z}_L^T\hat{\boldsymbol{F}}. \quad (129)$$

According to the orthogonality properties established in Section 3.3.2, see Equations (67)–(69), Equation (129) becomes diagonal, and the modal contribution for each i-th mode can be obtained from

$$[\mathrm{diag}(i\phi_i(\omega - \omega_i))]\boldsymbol{Q}(\omega) = \boldsymbol{Z}_L^T\hat{\boldsymbol{F}}, \quad (130)$$

yielding

$$Q_i(\omega) = \mathrm{i}\frac{\boldsymbol{z}_{L,i}^T\hat{\boldsymbol{F}}}{\phi_i(\omega_i - \omega)}. \quad (131)$$

Finally, the amplitude vector $\boldsymbol{Z}(\omega)$ can be expressed as

$$\boldsymbol{Z}(\omega) = \mathrm{i}\boldsymbol{Z}_R[\mathrm{diag}(\phi_i(\omega_i - \omega))]^{-1}\boldsymbol{Z}_L^T\hat{\boldsymbol{F}}. \quad (132)$$

For the particular problem of the charged mass considered in this study, if the eigenvectors have not been normalized in any specific way and take the form of Equations (57) and (59), the modal parameters ϕ_i result in

$$\begin{aligned} &\phi_1 = \tfrac{2im\alpha(\omega_2^2 - \omega_1^2)}{C}, \phi_2 = \tfrac{2im\beta(\omega_2^2 - \omega_1^2)}{C}, \\ &\phi_3 = -\phi_1, \phi_4 = -\phi_2. \end{aligned} \quad (133)$$

Then, the amplitudes $U_x(\omega)$ and $U_y(\omega)$ obtained by modal superposition are

$$U_x(\omega) = \frac{C}{m(\omega_2^2 - \omega_1^2)}\left[\frac{\omega_1 F_x + \mathrm{i}\alpha\omega F_y}{\alpha(\omega_1^2 - \omega^2)} + \frac{\beta\omega_2 F_x - \mathrm{i}\omega F_y}{(\omega_2^2 - \omega^2)}\right], \quad (134)$$

$$U_y = \frac{C}{m(\omega_2^2 - \omega_1^2)}\left[\frac{-\mathrm{i}\omega F_x + \alpha\omega_1 F_y}{(\omega_1^2 - \omega^2)} + \frac{\mathrm{i}\beta\omega F_x + \omega_2 F_y}{\beta(\omega_2^2 - \omega^2)}\right]. \quad (135)$$

Thanks to the state-space formulation, the amplitudes have been decomposed into the contribution of each mode. Similarly, the four FRFs can be decomposed into modal contributions, yielding

$$H_{xx}(\omega) = \frac{C}{m(\omega_2^2 - \omega_1^2)}\left[\frac{\omega_1}{\alpha(\omega_1^2 - \omega^2)} + \frac{\beta\omega_2}{\omega_2^2 - \omega^2}\right], \quad (136)$$

$$H_{xy}(\omega) = -H_{yx}(\omega) = \frac{-\mathrm{i}\omega C}{m(\omega_2^2 - \omega_1^2)}\left[\frac{-1}{\omega_1^2 - \omega^2} + \frac{1}{\omega_2^2 - \omega^2}\right], \quad (137)$$

$$H_{yy}(\omega) = \frac{C}{m(\omega_2^2 - \omega_1^2)}\left[\frac{\alpha\omega_1}{\omega_1^2 - \omega^2} + \frac{\omega_2}{\beta(\omega_2^2 - \omega^2)}\right]. \quad (138)$$

These expressions yield the same results as those obtained using the direct method in the configuration-space coordinates presented in the previous section. However, the modal approach offers the additional advantage of separating the total response into the individual contributions of each mode.

6 | Numerical Application

In this section, a numerical example is presented to illustrate some of the properties analyzed throughout the paper. For this

example, unit values are assigned to the parameters m, k_x, and to the product $q \times B$; that is, $m = 1\,\text{kg}$, $k_x = 1\,\text{N/m}$, and $C = qB/m = 1\,\text{rad/s}$. To obtain two angular frequencies related by an integer ratio, the value $k_y = 6.945\,\text{N/m}$ is selected. First, the natural frequencies and eigenvectors are computed. Then, a case of free vibrations is analyzed, examining the time response, its decomposition into modal contributions, and the energy transfer between the system degrees of freedom. Finally, the frequency response to a harmonic excitation is studied, with emphasis on its modal decomposition.

6.1 | Eigensolutions

The uncoupled angular natural frequencies are $\omega_x = 1\,\text{rad/s}$ and $\omega_y = 2.549\,\text{rad/s}$, while the coupled frequencies are $\omega_1 = 0.922\,\text{rad/s}$ and $\omega_2 = 2.765\,\text{rad/s}$. As expected, the lower frequency decreases and the higher one increases due to the coupling. The corresponding periods are $T_1 = 6.817\,\text{s}$ and $T_2 = 2.272\,\text{s}$, and since $T_1 = 3T_2$, the period of the resulting motion is T_1. The coefficients α and β of the eigenvectors are $\alpha = 0.163$ and $\beta = 0.416$, respectively. This confirms the previously established inequality $\beta > \alpha$.

6.2 | Free Vibration

In this free vibration example, the time response, its decomposition into modal contributions, and the energy transfer between the system degrees of freedom are analyzed. Let us consider the following initial conditions: $x_0 = 0$, $y_0 = 1\,\text{mm}$, $\dot{x}_0 = \dot{y}_0 = 0$. Either from Equation (95) or by (112), the response can be decomposed into the contribution of each mode, $\boldsymbol{u}(t) = \boldsymbol{u}_1(t) + \boldsymbol{u}_2(t)$, that is

$$\boldsymbol{u}(t) = \begin{Bmatrix} x(t) \\ y(t) \end{Bmatrix} = \begin{Bmatrix} x_1(t) \\ y_1(t) \end{Bmatrix} + \begin{Bmatrix} x_2(t) \\ y_2(t) \end{Bmatrix}, \tag{139}$$

where $x_1(t)$ and $y_1(t)$ correspond to the horizontal and vertical motions associated with the angular frequency ω_1, and $x_2(t)$ and $y_2(t)$ to those associated with ω_2. Figure 4 shows the responses $x(t)$ and $y(t)$, along with the individual contributions of each mode, over a time interval of $T_1 = 3T_2$. Specifically, Figure 4A represents the total response $x(t)$ and its decomposition into $x_1(t)$ and $x_2(t)$, and Figure 4B represents the total response $y(t)$ and its decomposition into $y_1(t)$ and $y_2(t)$.

Taking the initial conditions into account, the motion of the uncoupled system without mechanical-electrical-magnetic interaction would occur exclusively along the vertical axis, following a harmonic motion of angular frequency ω_y. In that case, only the second mode would be excited. However, due to coupling, mode 1 is also excited, and the vertical motion results from the superposition of both modes, with frequencies ω_1 and ω_2.

Figure 4B indicates that the dominant contribution to the vertical displacement $y(t)$ is provided by mode 2. It is worth noting that at $t = 0$, the initial position is not exclusively determined by the second mode, as would be expected in the uncoupled case. This is because, as previously discussed, the system lacks classical normal modes, and the modes cannot be excited independently. As a result, the initial displacement $y_0 = 1\,\text{mm}$ corresponds to 0.17 mm of mode 1 and to 0.83 mm of mode 2.

Mode coupling also affects the horizontal motion. Although the initial condition has no horizontal component, the velocity in the y direction generates a Lorentz force in the x direction, as shown in the free-body diagram in Figure 1B. Consequently, the horizontal and vertical motions are coupled, as illustrated by the $x(t)$ curve in Figure 4A. This horizontal response is the result of both modes, and as expected, the primary contribution is from the first mode.

This behavior exemplifies a fundamental consequence of the skew-symmetric electromagnetic coupling: modal responses become inseparable, and even initial conditions aligned with a single degree of freedom result in the excitation of both modes. The non-orthogonal nature of the eigenvectors implies that modal contributions are inherently entangled in both amplitude and phase. In particular, the imaginary parts of the mode shapes introduce fixed phase differences between the coordinates, which govern the motion. Although the system remains linear and conservative, the presence of non-normal modes gives rise to a qualitatively different vibrational behavior compared to classical self-adjoint systems.

This mode coupling can also be visualized using Lissajous curves, shown in Figure 5. These curves represent the in-plane

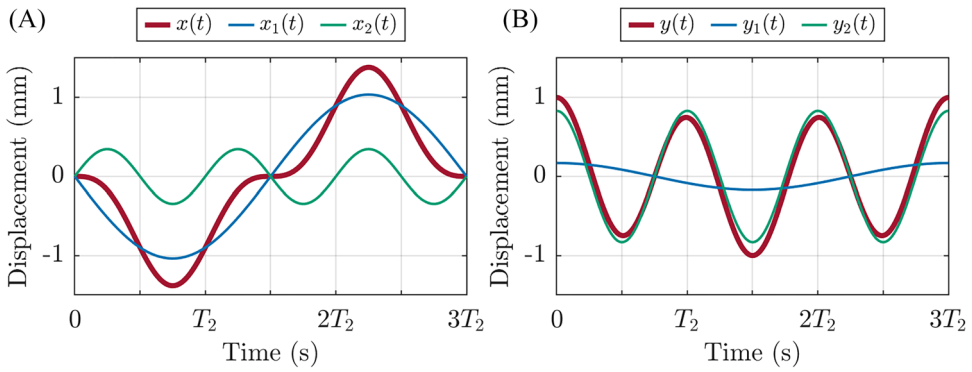

FIGURE 4 | Total response and decomposition into modes 1 and 2 of the free-vibration response of the charged mass under an applied magnetic field: (A) $x(t)$, $x_1(t)$, and $x_2(t)$; (B) $y(t)$, $y_1(t)$, and $y_2(t)$.

motion of the charged mass: the horizontal displacement $x(t)$ is plotted on the x-axis, and the vertical displacement $y(t)$ on the y-axis. The total motion is shown in Figure 5A, while the individual contributions of the modes 1 and 2 are shown in Figure 5B,C, respectively. The dot indicates the initial position. An animation of these curves is provided in Video S1 (Supporting Information).

The Lissajous curve in Figure 5A represents the trajectory described by the charged particle in the $x(t)$–$y(t)$ plane. The closed and symmetric shape indicates that the motion is bounded and periodic, consistent with the stable and conservative nature of the system. This curve corresponds to the case

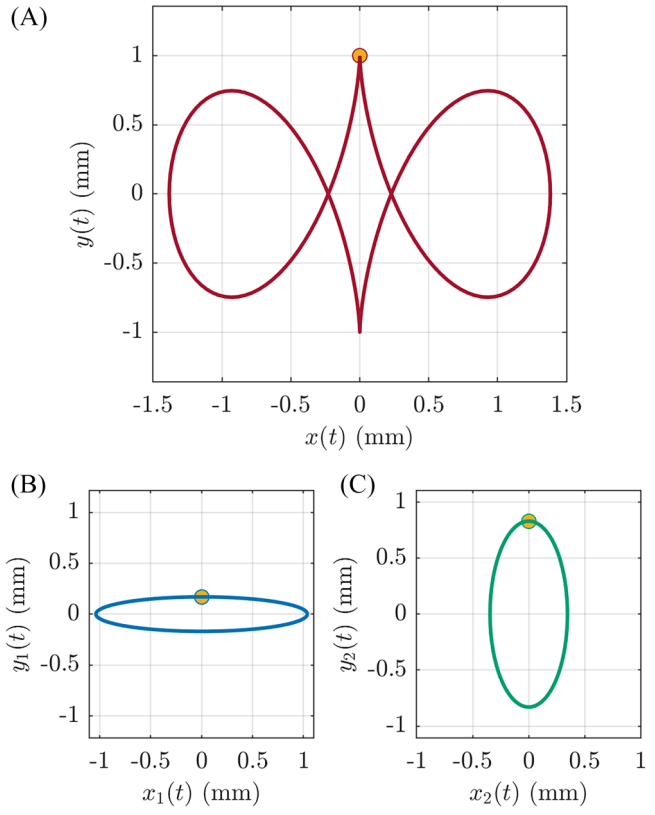

FIGURE 5 | Lissajous curves for the displacements $x(t)$ and $y(t)$: (A) total response $x(t) - y(t)$; (B) mode 1: $x_1(t) - y_1(t)$ and (C) mode 2: $x_2(t) - y_2(t)$.

$T_1 = 3T_2$, resulting in a regular pattern with two lateral lobes and a sharp vertical cusp.

Lissajous curves in Figure 5B,C display the individual contribution of modes 1 and 2, respectively. Figure 5B shows a horizontally elongated elliptical orbit, highlighting a dominant mode 1 in the x-direction. In contrast, Figure 5C presents a vertically oriented ellipse, where the amplitude is dominated by mode 2 in the y-direction.

It should be remarked the effect of mode coupling at the initial instant, as indicated by the red dots: the initial position $y_0 = 1$ mm in Figure 5A is decomposed into 0.17 mm for mode 1 (Figure 5B) and 0.83 mm for mode 2 (Figure 5C), as previously mentioned. From this instant onward, each oscillator follows a smooth, harmonic path, and the coupling introduces a fixed phase shift and continuous energy exchange, which are reflected in the geometric features of the combined trajectory. These effects are further illustrated in Figure 6.

Figure 6 illustrates the evolution of the system energy over time. Specifically, Figure 6A shows the kinetic energy $E_k(t)$, the potential energy $E_p(t)$, and the mechanical energy $E_m(t)$ (i.e., the sum of kinetic and potential energies) associated with the degree of freedom $x(t)$, while Figure 6B displays the corresponding energies for $y(t)$. Due to the quadratic nature of the energy functions, the period of the energy functions is half that of the displacement, namely, $T_1/2$ or $3T_2/2$. The total energy of the system is given by the yellow straight line, which corresponds to the potential energy initially stored in the vertical spring, $E_{\text{tot}} = 0.5k_y y_0^2 = 3.41$ μJ.

Figure 6A shows that the energy associated with $x(t)$ is zero at the initial time, since the body starts from rest at position y_0. However, as time progresses, energy transfer occurs due to the coupling, leading to an increase in the mechanical energy of $x(t)$, which splits into kinetic and potential components. This energy originates from the motion of $y(t)$, whose initial mechanical energy is the total energy of the system, as shown in Figure 6B. As time evolves, this energy undergoes an exchange between kinetic and potential forms and also transfers part of its energy to $x(t)$. The energy transferred between degrees of freedom up to an instant t is annotated in Figure 6A,B with $E_{\text{trans}}(t)$, i.e., the mechanical energy of $x(t)$, or the difference

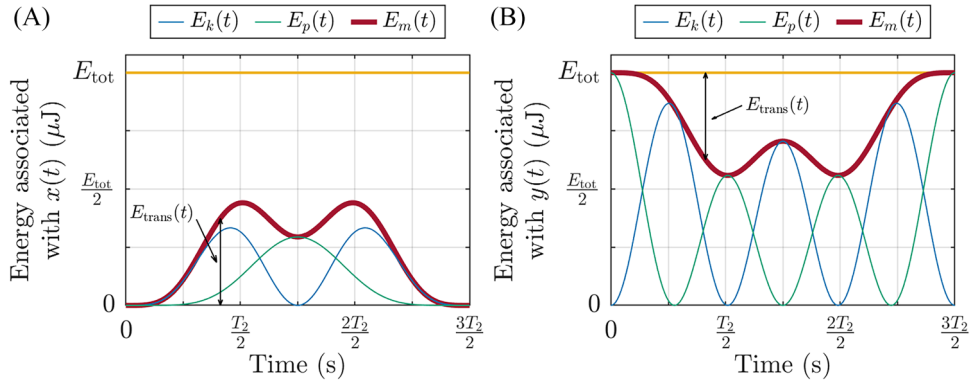

FIGURE 6 | Kinetic, potential, and mechanical energy of the system: (A) energy associated with the degree of freedom $x(t)$; (B) energy associated with the degree of freedom $y(t)$.

between the total energy of the system and the mechanical energy of $y(t)$.

This energy transfer is driven by the Lorentz forces depicted in the free-body diagram of Figure 1B. The power associated with the Lorentz force in the x-direction is $\dot{x}(t)qB\dot{y}(t)$, while the power in the y-direction is $-\dot{y}(t)qB\dot{x}(t)$. The fact that these powers have the same magnitude but opposite signs indicates that the energy lost by one degree of freedom is gained by the other. In other words, the net power is zero, and, as stated throughout this article, the system remains conservative. That is, the work done by the forces associated with the skew-symmetric coupling matrix $\mathbf{E}$ is zero.

Finally, the energy transferred between degrees of freedom up to any instant t is obtained from the integral of power as follows:

$$E_{\text{trans}}(t) = qB\int_0^t \dot{x}(\tau)\dot{y}(\tau)\mathrm{d}\tau. \tag{140}$$

This result matches the transferred energies annotated in Figure 6A,B. As conclusion, these results highlight the fundamental role of skew-symmetric coupling in the system energy: energy exchange is reversible, ensuring conservation while enabling dynamic coupling between modes. This mechanism underpins the non-orthogonal modal behavior observed in Figure 5 and distinguishes the system from classical modal frameworks.

6.3 | Frequency Response

In this numerical example, the frequency response to a harmonic excitation is studied, with emphasis on its modal decomposition. Let us consider the particular case of applying a unit force in the x direction, $F_x = 1$ N, and zero force in the y direction, $F_y = 0$. In this case, the amplitudes $U_x(\omega)$ and $U_y(\omega)$ are equivalent to the frequency response functions (FRFs) $H_{xx}(\omega)$ and $H_{yx}(\omega)$, respectively. The magnitude and phase of these functions are shown in Figure 7 as a function of the angular frequency ω for both the uncoupled and coupled cases. The FRFs obtained by the direct method are given by Equations (118) and (120), while those decomposed by modal superposition are given by Equations (136) and (137), respectively. The frequency range analyzed extends from zero to twice the second resonance frequency, $2\omega_2 = 5.53$ rad/s. Since the system is undamped, the response tends to infinity at the resonance frequencies. Therefore, the vertical axis in Figure 7 is limited to 100 m/N, although this value is not realistic, as any physical system would include damping, resulting in a finite response.

These figures show that in the uncoupled case, the direct receptance $H_{xx}(\omega)$ in Figure 7A exhibits a resonance peak at $\omega_x = 1$ rad/s, while the cross receptance $H_{yx}(\omega)$ is, as expected, zero, and thus is not shown in Figure 7B. When coupling is present, the resonance peak splits into two, corresponding to the eigenvalues $\omega_1 = 0.922$ rad/s and $\omega_2 = 2.765$ rad/s, previously determined in Section 6.1. It can be observed that, near each resonance, the magnitude curves of the individual modes coincide with the total response curve, indicating that the response is dominated by the corresponding mode in the vicinity of each resonance. In addition, an anti-resonance can be identified in $H_{xx}(\omega)$ at $\omega_y = 2.587$ rad/s, which is typical of a direct FRF.

Regarding the phase curves of the receptance functions, the phase of $H_{xx}(\omega)$ starts at 0° and alternates between 0° and 180° three times: once at each resonance frequency and once at the anti-resonance. In contrast, the phase of each individual modal contribution transitions from 0° to 180° at its corresponding resonance frequency. On the other hand, the phase of the cross receptance $H_{yx}(\omega)$ starts at −90° and alternates between −90° and 90° at the resonance frequencies. The phase of the contribution of mode 1 begins at −90°, while that of mode 2 begins at 90°, and each changes sign at its corresponding resonance. In all cases, due to modal coupling, the vibrations in the x and y directions exhibit a 90° phase difference. The anti-resonance and 90° phase shift in the cross responses underscore the nontrivial modal interactions induced by the coupling, despite the system being linear and conservative. The cross receptance aligns with the fixed phase relationship observed in the time-domain trajectories (Figure 5).

7 | Conclusions

In this paper, the mode coupling arising in a two-degree-of-freedom system with an electrostatically charged mass,

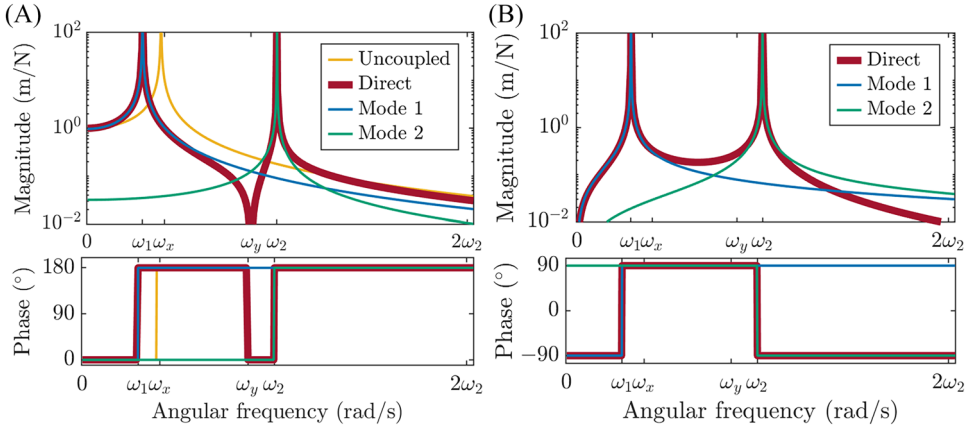

FIGURE 7 | Magnitude and phase of the FRFs obtained by the direct method and by modal superposition: (A) direct receptance $H_{xx}(\omega)$ and (B) cross receptance $H_{yx}(\omega)$.

resulting from the interaction between mechanical and electromagnetic fields, has been thoroughly analyzed. This study presents a minimal yet representative model of electromagnetic-mechanical coupling via a skew-symmetric matrix, capturing the essential dynamics in an analytically transparent manner. Its novelty lies in combining conceptual clarity with methodological completeness: the formulation isolates the effects of velocity-dependent conservative coupling—typically embedded in more elaborate systems—and explains their impact on modal behavior. The dual analysis in the configuration space and in the state space provides complementary perspectives and allows for both physical interpretation and formal modal decomposition.

The effects of this coupling on the eigenvalues and eigenvectors, the free vibration response, and the frequency response have been examined in detail, both in the configuration-space and in the state-space formulation. The most relevant conclusions are summarized below.

Eigenvalues and eigenvectors

- The eigenvalues of the coupled system are real. Compared to the uncoupled case, the smallest eigenvalue decreases, while the largest one increases.
- In the configuration space, the right and left eigenvectors form complex conjugate pairs. Their orthogonality properties are not straightforward, which prevents the application of classical modal superposition.
- In the state space, the size and number of eigenvectors are doubled, and they also appear as complex conjugate pairs. The left eigenvectors of the system $(\boldsymbol{B}, \boldsymbol{A})$ are the right eigenvectors of the system $(\boldsymbol{B}, \boldsymbol{A}^{\mathrm{T}})$. The first two components of the eigenvectors correspond to those in the configuration space.

Free vibration

- In the configuration space, the response is given by the superposition of undamped vibrations with angular frequencies determined by the eigenvalues. This response cannot be directly built from the eigenvectors and cannot be interpreted as a superposition of independent motions, since the system lacks normal modes.
- In the state space, the response can be constructed as the superposition of the eigenvectors weighted by their participation factors, through the use of orthogonality properties, although the eigenvectors correspond to "fictitious" modes.
- The numerical application has shown that the modes cannot be independently excited, since the eigenvectors are not orthogonal between them.

Frequency response

- In the configuration-space form, the number of variables and the size of the receptance matrix are smaller than in the state-space formulation, but this approach does not provide information about the contribution of each mode.
- The receptance matrix is not symmetric, suggesting energy transfer between modes.
- The numerical example has demonstrated the splitting of the single resonance peak of the uncoupled system into two distinct resonance peaks.

In summary, beyond its conceptual and methodological contributions, the presented analysis offers a useful reference for physical systems where nonsymmetric conservative coupling arises due to electromagnetic interactions. These include, for instance, magnetically suspended devices, vibration isolation systems, or energy harvesting structures with contactless actuation. Although intentionally simplified, the model captures essential dynamic phenomena—such as modal energy exchange and non-orthogonal behavior—that appear in more elaborate designs. As such, it provides a theoretical framework that may inform both analytical studies and control-oriented developments in electromechanical systems.

Acknowledgments

This study received financial support from the Department of Education of the Basque Government for the Research Group program IT1507–22.

Conflicts of Interest

The authors declare no conflicts of interest.

Data Availability Statement

Data sharing is not applicable to this article as no data sets were generated or analyzed during the current study.

References

1. M. Zhang, *Modeling of Multiphysics Electromagnetic & Mechanical Coupling and Vibration Controls Applied to Switched Reluctance Machine* (Université Paris Saclay, 2018), https://theses.hal.science/tel-02426016v2.

2. X. Chen, H. Wei, T. Deng, Z. He, and S. Zhao, "Investigation of Electromechanical Coupling Torsional Vibration and Stability in a High-Speed Permanent Magnet Synchronous Motor Driven System," *Applied Mathematical Modelling* 64 (2018): 235–248, https://doi.org/10.1016/j.apm.2018.07.030.

3. S. Wang, X. Zhao, Y. Xia, and J. Xiu, "Mechanical-Electromagnetic Coupling Elastic Vibration Instability of Symmetrical Three-Phase External Rotor Induction Motor," *Nonlinear Dynamics* 97, no. 1 (2019): 1–20, https://doi.org/10.1007/s11071-019-04901-1.

4. J. Dou, Z. Li, H. Yao, M. Ding, and G. Wei, "Torsional Vibration Suppression and Electromechanical Coupling Characteristics of Electric Drive System Considering Misalignment," *Applied Mathematics and Mechanics* 45 (2024): 1987–2010, Published Online May, https://doi.org/10.1007/s10483-024-3179-6.

5. A. Belahcen, R. Kouhia, and K. Fonteyn, "The Different Levels of Magneto-Mechanical Coupling in Energy Conversion Machines and Devices," in *IV International Conference on Computational Methods for Coupled Problems in Science and Engineering*, ed. M. Papadrakakis, E. Oñate, and B. Schrefler (CIMNE, 2011), 472–483.

6. Y. Chen, X. Xing, F. Sun, and J. Lin, "Electromagnetic-Mechanical Coupling Analysis and Optimization Method of Electromagnetic Vibroseis," *Measurement Science and Technology* 34, no. 9 (2023): 095901, https://doi.org/10.1088/1361-6501/accfb6.

7. F. Cortés, O. Zarraga, I. Sarría, and M. J. Elejabarrieta, "Eddy Currents Damping Understood as Zener Viscoelastic Damping," *Journal of Sound and Vibration* 547 (2023): 117539, https://doi.org/10.1016/j.jsv.2022.117539.

8. J. Li and G. Yang, "Equivalent Subdomain Method for Performance Prediction of Permanent Magnet Eddy Current Brakes," *IET Electric Power Applications* 15, no. 9 (2021): 1174–1186, https://doi.org/10.1049/elp2.12087.

9. Z. Lu, B. Huang, Q. Zhang, and X. Lu, "Experimental and Analytical Study on Vibration Control Effects of Eddy-Current Tuned Mass Dampers Under Seismic Excitations," *Journal of Sound and Vibration* 421 (2018): 153–165, https://doi.org/10.1016/j.jsv.2017.10.035.

10. B. Yan, Z. Wang, H. Ma, H. Bao, K. Wang, and C. Wu, "A Novel Lever-Type Vibration Isolator With Eddy Current Damping," *Journal of Sound and Vibration* 494 (2021): 115862, https://doi.org/10.1016/j.jsv.2020.115862.

11. B. Yan, N. Yu, and C. Wu, "A State-of-the-Art Review on Low-Frequency Nonlinear Vibration Isolation With Electromagnetic Mechanisms," *Applied Mathematics and Mechanics* 43, no. 7 (2022): 1045–1062, https://doi.org/10.1007/s10483-022-2868-5.

12. E. Diez-Jimenez, R. Rizzo, M. J. Gómez-García, and E. Corral-Abad, "Review of Passive Electromagnetic Devices for Vibration Damping and Isolation," *Shock and Vibration* 2019 (2019): 1250707, https://doi.org/10.1155/2019/1250707.

13. N. Yu, X. Fei, C. Wu, and B. Yan, "Modeling and Analysis of Magnetic Spring Enhanced Lever-Type Electromagnetic Energy Harvesters," *Applied Mathematics and Mechanics* 43, no. 5 (2022): 743–760, https://doi.org/10.1007/s10483-022-2849-9.

14. Z. Li, S. Zhou, and Z. Yang, "Recent Progress on Flutter-Based Wind Energy Harvesting," *International Journal of Mechanical System Dynamics* 2, no. 1 (2022): 82–98, https://doi.org/10.1002/msd2.12035.

15. G. Xu, C. Li, C. Chen, J. Fu, T. Hou, and Y. Zi, "Dynamics of Triboelectric Nanogenerators: A Review," *International Journal of Mechanical System Dynamics* 2, no. 4 (2022): 311–324, https://doi.org/10.1002/msd2.12058.

16. X. Guo, R. Avila, Y. Huang, and Z. Xie, "Flexible Electronics With Dynamic Interfaces for Biomedical Monitoring, Stimulation, and Characterization," *International Journal of Mechanical System Dynamics* 1, no. 1 (2021): 52–70, https://doi.org/10.1002/msd2.12017.

17. A. Z. Hajjaj, N. Jaber, S. Ilyas, F. K. Alfosail, and M. I. Younis, "Linear and Nonlinear Dynamics of Micro and Nano-Resonators: Review of Recent Advances," *International Journal of Non-Linear Mechanics* 119 (2020): 103328, https://doi.org/10.1016/j.ijnonlinmec.2019.103328.

18. L. A. Martinez, A. R. Castelli, W. Delmas, J. E. Sharping, and R. Chiao, "Electromagnetic Coupling to Centimeter-Scale Mechanical Membrane Resonators via RF Cylindrical Cavities," *New Journal of Physics* 18, no. 11 (2016): 113015, https://doi.org/10.1088/1367-2630/18/11/113015.

19. M. Cui, H. Liu, H. Jiang, Y. Zheng, X. Wang, and W. Liu, "Active Vibration Optimal Control of Piezoelectric Cantilever Beam With Uncertainties," *Measurement and Control* 55 (2022): 359–369, Published online, https://doi.org/10.1177/00202940221091244.

20. M. Kumar, B. Mukherjee, and S. Sen, "Analysis of Static Charge Induced Pull-In of an Electrostatic MEMS," *Communications in Nonlinear Science and Numerical Simulation* 96 (2021): 105690, https://doi.org/10.1016/j.cnsns.2021.105690.

21. Y. Yang, N. Zhang, H. Liu, J. Ling, and Z. Tan, "Piezoelectric and Flexoelectric Effects of DNA Adsorbed Films on Microcantilevers," *Applied Mathematics and Mechanics* 44, no. 9 (2023): 1547–1562, https://doi.org/10.1007/s10483-023-3026-5.

22. A. S. Nemov, M. K. Matikainen, T. Wang, and A. Mikkola, "Analysis of Electromechanical Systems Based on the Absolute Nodal Coordinate Formulation," *Acta Mechanica* 233, no. 3 (2022): 1019–1030, https://doi.org/10.1007/s00707-022-03153-2.

23. K. G. Aktaş and İ. Esen, "Dynamic Response Analysis and Active Vibration Control of the Smart Sandwich Composite Plate With FGM Core Layers and MIMO FGPM Actuators and Sensors," *International Journal of Mechanical System Dynamics* 5 (2025): 3–19, Published online March 1, https://doi.org/10.1002/msd2.70001.

24. T. S. Amer, F. M. El-Sabaa, S. K. Zakria, and A. A. Galal, "The Stability of 3-DOF Triple-Rigid-Body Pendulum System Near Resonances," *Nonlinear Dynamics* 110, no. 2 (2022): 1339–1371, https://doi.org/10.1007/s11071-022-07722-x.

25. T. S. Amer, G. M. Moatimid, S. K. Zakria, and A. A. Galal, "Vibrational and Stability Analysis of Planar Double Pendulum Dynamics Near Resonance," *Nonlinear Dynamics* 112, no. 24 (2024): 21667–21699, https://doi.org/10.1007/s11071-024-10169-x.

26. T. S. Amer, S. A. Abdelhfeez, R. F. Elbaz, and M. K. Abohamer, "Investigation of the Dynamical Analysis, Stability, and Bifurcation for a Connected Damped Oscillator With a Piezoelectric Harvester," *Journal of Vibration Engineering & Technologies* 13, no. 2 (2025): 155, https://doi.org/10.1007/s42417-024-01641-4.

27. T. S. Amer, E. H. Aly, and H. M. Gad, "Analysis and Stability Assessment of the Vibratory Motion of a Magnetic Mechanical System Near Resonance," *Journal of Vibration Engineering & Technologies* 13, no. 3 (2025): 201, https://doi.org/10.1007/s42417-024-01629-0.

28. G. M. Moatimid, T. S. Amer, and M. H. Zekry, "Analytical and Numerical Study of a Vibrating Magnetic Inverted Pendulum," *Archive of Applied Mechanics* 93, no. 6 (2023): 2533–2547, https://doi.org/10.1007/s00419-023-02395-3.

29. G. M. Moatimid and T. S. Amer, "Analytical Approximate Solutions of a Magnetic Spherical Pendulum: Stability Analysis," *Journal of Vibration Engineering & Technologies* 11, no. 5 (2023): 2155–2165, https://doi.org/10.1007/s42417-022-00693-8.

30. R. R. Craig Jr. and A. J. Kurdila, "Vibration Properties of MDOF Systems: Modes, Frequencies, and Damping," in *Fundamentals of Structural Dynamics*, 2nd ed. (John Wiley & Sons Inc., 2006), 281–324.

31. W. Wang and J. Kirkhope, "New Eigensolutions and Modal Analysis for Gyroscopic/Rotor Systems, Part 1: Undamped Systems," *Journal of Sound and Vibration* 175, no. 2 (1994): 159–170, https://doi.org/10.1006/jsvi.1994.1320.

32. W. Wang and J. Kirkhope, "New Eigensolutions and Modal Analysis for Gyroscopic/Rotor Systems, Part 2: Perturbation Analysis for Damped Systems," *Journal of Sound and Vibration* 175, no. 2 (1994): 171–183, https://doi.org/10.1006/jsvi.1994.1321.

33. S. Adhikari, "Modal Analysis of Linear Asymmetric Non-conservative Systems," *Journal of Engineering Mechanics* 125, no. 12 (1999): 1372–1379, https://doi.org/10.1061/(ASCE)0733-9399(1999)125:12(1372).

Supporting Information

Additional supporting information can be found online in the Supporting Information section.
Video 1.